

The pre-eruptive magma plumbing system of the 2007–2008 dome-forming eruption of Kelut volcano, East Java, Indonesia

A. J. Jeffery · R. Gertisser · V. R. Troll · E. M. Jolis ·
B. Dahren · C. Harris · A. G. Tindle · K. Preece ·
B. O'Driscoll · H. Humaida · J. P. Chadwick

Received: 30 October 2012 / Accepted: 19 March 2013 / Published online: 17 April 2013
© Springer-Verlag Berlin Heidelberg 2013

Abstract Kelut volcano, East Java, is an active volcanic complex hosting a summit crater lake that has been the source of some of Indonesia's most destructive lahars. In November 2007, an effusive eruption lasting approximately 7 months led to the formation of a 260-m-high and 400-m-wide lava dome that displaced most of the crater lake. The 2007–2008 Kelut dome comprises crystal-rich basaltic andesite with a texturally complex crystal cargo of strongly zoned and in part resorbed plagioclase (An_{47-94}), orthopyroxene (En_{64-72} , Fs_{24-32} , Wo_{2-4}), clinopyroxene (En_{40-48} , Fs_{14-19} , Wo_{34-46}), Ti-magnetite (Usp_{16-34}) and trace amounts of apatite, as well as ubiquitous glomerocrysts of varying magmatic mineral assemblages. In addition, the notable occurrence of magmatic and crustal

xenoliths (meta-basalts, amphibole-bearing cumulates, and skarn-type calc-silicates and meta-volcaniclastic rocks) is a distinct feature of the dome. New petrographical, whole rock major and trace element data, mineral chemistry as well as oxygen isotope data for both whole rocks and minerals indicate a complex regime of magma-mixing, decompression-driven resorption, degassing and crystallisation and crustal assimilation within the Kelut plumbing system prior to extrusion of the dome. Detailed investigation of plagioclase textures alongside crystal size distribution analyses provide evidence for magma mixing as a major pre-eruptive process that blends multiple crystal cargoes together. Distinct magma storage zones are postulated, with a deeper zone at lower crustal levels or near the crust-mantle boundary (>15 km depth), a second zone at mid-crustal levels (~10 km depth) and several magma storage zones distributed throughout the uppermost crust (<10 km depth). Plagioclase-melt and amphibole hygrometry indicate magmatic H_2O contents ranging from ~8.1 to 8.6 wt.% in the lower crustal system to ~1.5 to

Communicated by J. Hoefs.

Electronic supplementary material The online version of this article (doi:10.1007/s00410-013-0875-4) contains supplementary material, which is available to authorized users.

A. J. Jeffery (✉) · R. Gertisser · B. O'Driscoll
School of Physical and Geographical Sciences, Keele University,
Keele, Staffordshire ST5 5BG, UK
e-mail: a.j.jeffery@keele.ac.uk

V. R. Troll · E. M. Jolis · B. Dahren
Department of Earth Sciences, Centre for Experimental
Mineralogy, Petrology and Geochemistry (CEMPEG), Uppsala
University, Villavägen 16, 752 36 Uppsala, Sweden

C. Harris
Department of Geological Science, University of Cape Town,
Rondebosch, Cape Town 7701, South Africa

A. G. Tindle
CEPSAR (Centre for Earth, Planetary, Space and Astronomy
Research), The Open University, Walton Hall, Milton Keynes
MK7 6AA, UK

K. Preece
School of Environmental Sciences, University of East Anglia,
Norwich NR4 7TJ, UK

H. Humaida
Balai Penyelidikan dan Pengembangan Teknologi
Kegunungapian, Yogyakarta 55166, Indonesia

J. P. Chadwick
Science Gallery, Trinity College Dublin, Pearse Street,
Dublin 2, Ireland

3.3 wt.% in the mid to upper crust. Pyroxene and plagioclase $\delta^{18}\text{O}$ values range from 5.4 to 6.7 ‰, and 6.5 to 7.6 ‰, respectively. A single whole rock analysis of the 2007–2008 dome lava gave a $\delta^{18}\text{O}$ value of 7.6 ‰, whereas meta-basaltic and calc-silicate xenoliths are characterised by $\delta^{18}\text{O}$ values of 6.2 and 10.3 ‰, respectively. Magmatic $\delta^{18}\text{O}$ values calculated from individual pyroxene and plagioclase analyses range from 5.7 to 7.0 ‰, and 6.2 to 7.4 ‰, respectively. This range in O-isotopic compositions is explained by crystallisation of pyroxenes in the lower to mid-crust, where crustal contamination is either absent or masked by assimilation of material having similar $\delta^{18}\text{O}$ values to the ascending melts. This population is mixed with isotopically distinct plagioclase and pyroxenes that crystallised from a more contaminated magma in the upper crustal system. Binary bulk mixing models suggest that shallow-level, recycled volcanoclastic sedimentary rocks together with calc-silicates and/or limestones are the most likely contaminants of the 2007–2008 Kelut magma, with the volcanoclastic sediments being dominant.

Keywords Kelut volcano · Sunda arc · Lava dome · CSD · Oxygen isotopes · Magma mixing · Crustal contamination · Volcanic hazards

Introduction

Kelut volcano, East Java (Fig. 1), is one of the most hazardous volcanoes in Indonesia due to its unpredictable style of eruption and its capacity to generate devastating syn-eruptive lahars (Bourdier et al. 1997; van Bergen et al. 2000; Siebert et al. 2011). The eruptive history of Kelut has been dominated by plinian and phreatomagmatic eruption styles (Siebert et al. 2011), the latest of which occurred in 1990 (Bourdier et al. 1997). However, in 2007, an effusive eruption lasting approximately 7 months generated a new lava dome within the summit crater that protruded from and eventually displaced the active crater lake (Jeffery et al. 2010). This latest, and in many respects, unusual eruption of Kelut was in stark contrast with the preceding six eruptions, which were dominantly short-lived, explosive events of VEI between 3 and 5 (Siebert et al. 2011), and unpredicted by volcanologists and local authorities. Like other lava domes at andesite volcanoes (e.g. Merapi, Indonesia; Colima, Mexico; Montserrat, Lesser Antilles; Shiveluch, Kamchatka), the 2007–2008 lava dome of Kelut contains a diverse mineral assemblage, including complexly zoned crystals, glomerocrysts of varying mineralogical assemblages as well as a range of magmatic and crustal xenoliths that are indicative of a complex regime of pre-eruptive processes, involving fractional crystallisation,

magma mixing and mingling, crystal recycling, decompression-induced crystallisation and crustal contamination (cf. Davidson and Tepley 1997; Tepley et al. 2000; Blundy and Cashman 2001; Cooper and Reid 2003; Gamble et al. 2003; Price et al. 2005; Annen et al. 2006; Humphreys et al. 2006; Martin et al. 2006; Chadwick et al. 2007, 2013; Reubi and Blundy 2008; Dahren et al. 2012; Gardner et al. 2013; Troll et al. 2013).

The aims of this study are to (1) place constraints upon the main magma storage zones beneath Kelut volcano, (2) identify pre-eruptive magmatic processes occurring within the magma plumbing system, (3) evaluate the conditions

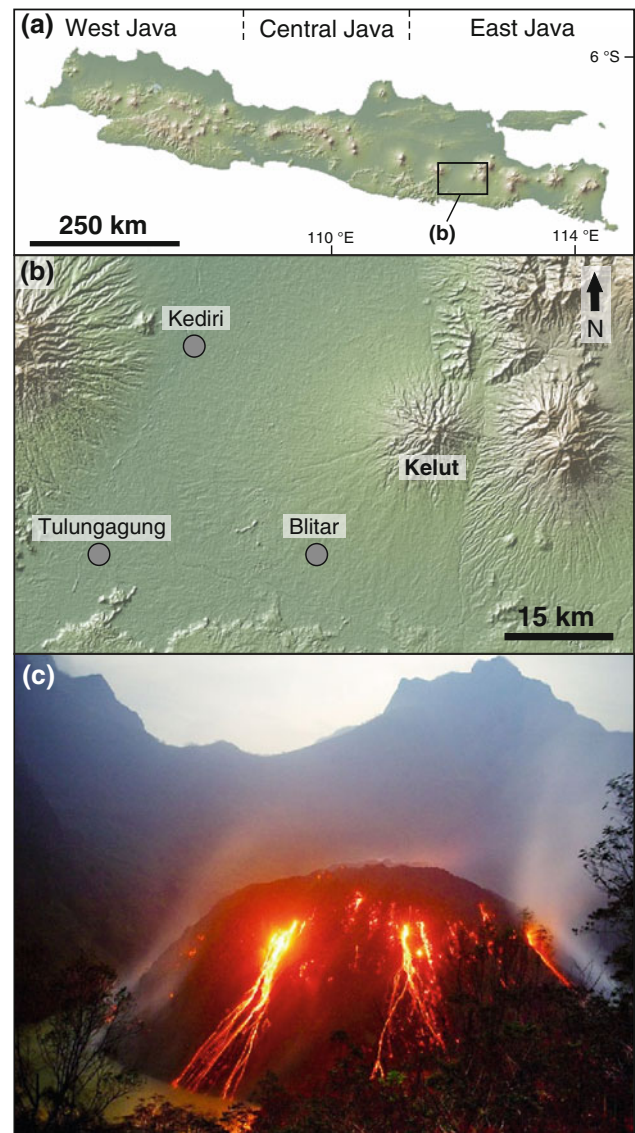


Fig. 1 a Location map showing major volcanoes and geographical divisions of Java, Indonesia b Map showing Kelut, the local topography and nearby major settlements c Photograph of the active Kelut 2007–2008 lava dome, with permission and courtesy of Tom Pfeiffer. All maps were generated using GeoMapApp©

and processes that lead to a change from explosive activity at Kelut, as exemplified by the penultimate eruption in 1990, to lava dome extrusion in 2007–2008, and (4) assess the role of crustal contamination at Kelut and other volcanoes in East Java. These aims are addressed through a combination of petrography, thermobarometry and quantitative textural analysis, as well as major element, trace element and oxygen isotope geochemistry of the 2007–2008 Kelut lava dome, its crystal cargo and its magmatic and crustal xenoliths. Four samples of pyroclastic material from the preceding explosive eruption in 1990 are included for comparative purposes to evaluate the potential effect of magma compositions on eruption style.

Geodynamic setting, geology and eruptive history of Kelut volcano

Kelut is part of the Quaternary volcanic front of the active Sunda arc system, a 5,600-km-long volcanic chain that extends from the Andaman Islands (north-west of Sumatra) to the Banda Arc in the East (van Bemmelen 1949; Hamilton 1979; Newcomb and McCann 1987; Hilton and Craig 1989; Widiyantoro and van der Hilst 1996). The Sunda and Banda arcs mark a convergent boundary between the Indo-Australian Plates and the Eurasian Plate (Hamilton 1979; Silver et al. 1983). The boundary itself is marked by a major trench, the Java Trench, where the Indo-Australian Plates are subducting northwards beneath the Sunda Arc (Hamilton 1979; Newcomb and McCann 1987). Kelut volcano overlies 8–11 km of reworked, volcanoclastic crustal sediments, overlain by shallow crustal limestones. Beneath this, the Cretaceous basement is considered to comprise arc/ophiolite material (Smyth et al. 2005 and references therein).

Kelut is a basaltic andesite stratovolcano with a summit elevation of 1,731 m, ~27 km east of the city of Kediri in East Java (Fig. 1a, b) (Wirakusumah 1991; Lesage and Surono 1995; van Bergen et al. 2000; De Bézilal et al. 2012). It is located on the west side of the Kawi–Laksono–Anjasmoro volcanic range and comprises two landslide (sector collapse) scars derived from previous slope failures (Thouret et al. 1998). The eastern caldera opens to the south and is currently dormant. The western caldera contains the lake-filled, active crater of Kelut and preserved remnants of several older lava domes (Bourdier et al. 1997). The western slopes comprise mainly debris avalanche deposits. These are overlain by scoria- and block-rich pyroclastic flow deposits that grade into debris flows (lahars) with increasing distance from the summit (Thouret et al. 1998).

Over the past 1,000 years, Kelut has erupted 32 times (Siebert et al. 2011). Seven eruptions have occurred since

A.D. 1900 (Lesage and Surono 1995; Siebert et al. 2011), and due to the presence of a large crater lake (known to have reached $7.8 \times 10^7 \text{ m}^3$ in volume in 1875; van Bergen et al. 2000), the current crater complex is infamous for its capacity to produce some of the world's most destructive lahars. These include primarily syn-eruptive, hot lahars caused by activity in the crater lake, although secondary (post-eruptive) lahars caused by heavy rainfall onto Kelut's unconsolidated flanks have also occurred (Siebert et al. 2011). In 1586, the most devastating of these lahars caused ~10,000 fatalities (van Bergen et al. 2000). The western crater rim has been lowered by a series of wall collapses during the 1848 and 1875 eruptive events, allowing for devastating lake outbursts (Lavigne et al. 2007). The western flank of the volcano is therefore most commonly affected by lahars, transporting debris to the lowland plains around Kediri, Tulungagung and Blitar (Fig. 1b), three cities that cumulatively account for >160,000 inhabitants (Thouret et al. 1998). The devastating lahars associated with the 1919 eruption resulted in >5,000 fatalities and prompted the drilling of several tunnels through the western crater wall in an attempt to drain the crater lake. Although complications delayed the project until 1926, it proved to be successful, lowering the crater lake volume to $\sim 2 \times 10^6 \text{ m}^3$ (Bourdier et al. 1997; van Bergen et al. 2000). Prior to the 1990 eruption, the crater was filled again by a $\sim 2.5 \times 10^6 \text{ m}^3$ lake (Bourdier et al. 1997), but the lake was displaced entirely during the 1990 eruption, revealing a small (tens of metres high) embryonic lava dome. Continued activity since then took the form of lake re-establishment, fumaroles, secondary lahars and, immediately prior to the 2007–2008 eruption, an increase in crater lake temperature. Following 1990, continuous monitoring revealed that the lake level was rising as much as 5 cm in a single day and could potentially refill entirely within a single year. Before the 2007–2008 events commenced, the crater lake was ~34 m deep, ~350 m in diameter and contained once more $\sim 2.1 \times 10^6 \text{ m}^3$ of water (Siebert et al. 2011).

The 2007–2008 eruption of Kelut volcano

On 11 September 2007, changes in the colour and temperature of the crater lake water prompted the Ministry of Energy and Mineral Resources and the Centre of Volcanology and Geological Hazard Mitigation (CVGHM) to advise an off-limits zone within 5 km of the lake. About 4 months prior to this, echo sounding and floating accumulation chamber studies identified anomalous CO_2 fluxes throughout 2007 compared to previous years (Caudron et al. 2012). On 11 September, the total flux of CO_2 was noted to reach values in excess of 500 tons/day, more than

ten times greater than measurements taken in 2005 and 2006 (Siebert et al. 2011). Crater lake chemistry and temperatures continued to change throughout September and October 2007, alongside increased seismic activity and deformation, prompting an evacuation of villages within 10 km of the crater and the temporary displacement of ~50,000 people (Siebert et al. 2011).

By 4 November 2007, the lake water had reached temperatures of 50 °C and white plumes of steam were observed rising from the crater (~2 km above the crater). A number of shallow earthquakes were recorded, and video footage from within the crater revealed a large black mass of rock that protruded from the crater lake on 4 November. The growth of a lava dome surprised local authorities, who were expecting an explosive eruption similar in style to the 1990 events (Bourdier et al. 1997; De Bézilal et al. 2012). Steam plumes of varied size were continually emitted throughout November (one plume reached 3.7 km altitude on 11 November), and by early December 2007, the lake water temperature reached 75 °C. The height of the lava dome was then measured as 120 m above lake level and ~250 m in diameter at the same marker. Surface temperatures of the dome rock were recorded between 150 and 210 °C at that point (Siebert et al. 2011).

The lava dome remained active throughout November and December 2007, although with progressively reduced seismic activity. The next 6 months, until 9 June 2008, saw occasional steam plumes rising to ~50 to 150 m above the crater (Siebert et al. 2011), and by 12 May 2008, the crater lake was almost entirely depleted. Water within the local drainage system (~960 m away from the dome) reached temperatures >65 °C at this stage. By May 2008, the lava dome was considered to have stopped growing, having reached an estimated size of ~260 m in height, ~400 m in width at its base and $3.5 \times 10^7 \text{ m}^3$ in volume (Siebert et al. 2011). Activity since May 2008 has taken the form of occasional diffuse white plumes rising from the dome.

Methodology

Analytical techniques

Whole rock major and trace element analyses of the 2007–2008 lava dome (samples KLT-K2, KLT-71a, KLT-K3, KLT-A) and additional samples of pyroclastic material deposited during the 1990 eruption (samples KLT-901, KLT-902, KLT-903, KLT-904) were undertaken at Acme Analytical Laboratories Ltd, Canada, using inductively coupled plasma atomic emission spectroscopy (ICP-AES) for major element analysis and inductively coupled plasma mass spectrometry (ICP-MS) for trace element analysis. Weathered surfaces and visible xenoliths were removed

from samples prior to crushing in an agate mill. Samples were dried at 60 °C prior to mixing with a $\text{LiBO}_2/\text{Li}_2\text{B}_4\text{O}_7$ flux and dilute nitric digestion. Loss-on-ignition was reported as weight difference after ignition for 2 h at 1,000 °C. Base metals (Cu, Mo, Ni, Pb, Zn) were determined from samples that were digested in Aqua Regia. Detection limits of trace elements were typically between 0.1 and 1 ppm, depending upon the element. Data quality was monitored using a set of certified internal reference materials.

Additional whole rock major element analyses of the 2007–2008 dome lava (K-A1A, K-L-6, K-A-1) and xenoliths contained therein (samples K-L + XC-1, K-L + XC-4, K-L + XC-9) were undertaken using a Philips PW 2400 X-ray fluorescence spectrometer at Vrije Universiteit Amsterdam (VU), the Netherlands. Samples were crushed in an agate mill and dried, before being heated to generate fused glass beads. Major element contents were calibrated using international reference standards, and in-house standards were used as internal monitors.

Major element compositions of plagioclase, clinopyroxene, orthopyroxene, amphibole and Fe–Ti oxides were analysed using a CAMECA SX 100 electron microprobe at The Open University, UK, and a JEOL JXA-8200 Superprobe at Vrije Universiteit. Peak counting times per element were 12.5–25 s using a 10- μm defocused beam, an acceleration voltage of 20 kV and a beam current of 20–27 nA. Major elements and volatiles (Cl and S) in groundmass glass and plagioclase-hosted melt inclusions were determined using a JEOL JXA 8900 RL electron microprobe at the University of Göttingen, Germany. Peak counting times ranged from 15 to 30 s for major elements and 30 s for volatiles, using a 10- μm defocused beam, an acceleration voltage of 15 kV and a beam current of 15 nA. Detection limits for Cl and S were ~45 and ~115 ppm, respectively (A. Kronz pers. comm. 2011). Natural silicate minerals and pure metals were used as primary standards to calibrate the instrument. Silicate mineral and volcanic glass standards (VG-568, KN-18 and KE-12) were routinely analysed as secondary standards.

Oxygen–isotope ratios of whole rock samples were determined at the University of Cape Town (UCT), South Africa, by conventional techniques, whilst orthopyroxene, clinopyroxene and plagioclase separates were analysed by laser fluorination. Samples were crushed in a jaw crusher, and minerals or rock fragments were hand-picked from the crushed materials under a stereo-binocular microscope, making sure that only pristine materials were used for analysis. Powders for conventional oxygen isotope analysis were produced from the sand-sized crush via an agate ball mill. Approximately 10 mg of sample was reacted with ClF_3 and the liberated O_2 converted to CO_2 using a hot platinised carbon rod. Further details of the extraction

methods for oxygen from silicates employed at UCT have been given by Vennemann and Smith (1990) and Fagereng et al. (2008). For samples K-L-XP-6 and K-A-1, pyroxenes and plagioclase were analysed by laser fluorination following the method described by Harris and Vogeli (2010). Each sample was reacted in the presence of ~ 10 kPa BrF_5 , and the purified O_2 was collected onto a 5\AA molecular sieve contained in a glass storage bottle. All O-isotope ratios were measured offline using a Finnegan DeltaXP mass spectrometer. The results are reported in standard δ -notation, $\delta = (R_{\text{sample}}/R_{\text{standard}} - 1) \times 1,000$, relative to SMOW (Standard Mean Ocean Water). For the conventional method, samples were run in batches of eight, along with duplicate samples of the internal quartz standard NBS-28 ($\delta^{18}\text{O} = 9.64$ ‰). During the course of this study, the analytical error for $\delta^{18}\text{O}$ is estimated to be ± 0.1 ‰ (1σ) based on long-term duplication of NBS-28. The O-isotope ratios of samples analysed using laser fluorination were measured on O_2 gas. Measured values of the internal standard MON GT (Harris et al. 2000) were used to normalise the raw data and correct for drift in the reference gas. The long-term average difference on $\delta^{18}\text{O}$ values of duplicates of MON GT analysed is 0.13 ‰ and corresponds to a 2σ value of 0.16 ‰.

Crystal size distribution analysis

To generate crystal size distributions (CSDs) for the Kelut dome rocks, high-resolution photomicrographs were taken and digitally joined to create single thin-section texture maps. These images were imported into a vector graphics editor, allowing the identification and digitisation of individual crystals. Vesicles were also digitised to allow calculation of vesicularity. For groundmass microlite CSDs, BSE images were stitched together to create a single, high-resolution image with an adequate number of crystals for CSD analysis. Digitised images were exported as greyscale tiff format images and imported into *ImageJ*, where best-fit ellipses were applied to determine long- and short-axis measurements. Mean crystal aspect ratios were calculated using the *CSDSlice* methodology of Morgan and Jerram (2006). These were used as inputs for the program *CSD-Corrections 1.39* (Higgins 2000) to generate CSDs. All CSDs were calculated using a minimum of 200 crystals (Mock and Jerram 2005; Morgan and Jerram 2006). Samples were classified as massive (lacking mineral alignment) and given an approximate crystal roundness of 0.3, based on a scale of 0 (angular) to 1 (spherical), with 5 bins per decade. The total slide area, volumetric phase abundance and vesicularity were calculated using image processing software (*ImageJ* and *ImageTool*), to provide a scale and allow accurate measurement of the CSD before vesiculation. Where CSD slopes were curved or kinked, individual

segments were interpreted using least squares regression calculated using Microsoft Excel. The maximum length (L_{max}) was calculated by averaging the largest four crystals within each population (Boorman et al. 2004).

Plagioclase-melt thermometry/hygrometry

The recognition of distinctive relationships between plagioclase composition and parameters such as temperature, pressure and $\text{H}_2\text{O}_{\text{melt}}$, combined with the relative abundance of plagioclase within igneous rocks, has led to the development of plagioclase-melt geothermobarometers and hygrometers during the last 40 years (e.g. Kudo and Weill 1970; Drake 1976; Loomis 1979; Glazner 1984; Housh and Luhr 1991; Putirka 2005, 2008; Lange et al. 2009). Whilst the reliability of plagioclase-melt barometry is not well constrained (Putirka 2008), the recalibrated form of the models of Sugawara (2001) and Ghiorso et al. (2002) provides thermometers that can be applied to hydrous systems, but requires an estimate of $\text{H}_2\text{O}_{\text{melt}}$ [standard error of estimate (SEE) ± 36 °C] (Putirka 2008, equation 24a). This model will be referred to as P08-24a and has been applied to the dome lava plagioclase population, in addition to two hygrometers; model H of Putirka (2005) (SEE ± 1.2 wt.% and referred to here as P05-mH) and equation 25b of Putirka (2008) (SEE ± 1.1 wt.% and referred to here as P08-25b). It should be noted that P08-25b is considered to be more accurate than P05-mH for $\text{H}_2\text{O}_{\text{melt}}$ values.

Clinopyroxene-melt thermobarometry

Two clinopyroxene-melt models have been used to calculate pre-eruptive P–T conditions. The first allows the determination of temperature and pressure for hydrous melts using jadeite-diopside/hedenbergite exchange equilibria (Putirka et al. 2003). This model (here referred to as P03) is considered one of the most versatile of those currently available (SEE of ± 33 °C and ± 170 MPa) and has been applied successfully to numerous studies aimed at constraining intensive parameters for magma plumbing systems (e.g. Schwarz et al. 2004; Longpré et al. 2008; Stroncik et al. 2009; Hildner et al. 2011; Barker et al. 2012; Dahren et al. 2012).

The second model is based upon the partitioning of Al between clinopyroxene and melt and is calibrated for hydrous systems also (Putirka 2008, equation 32c). This model (here referred to as P08-32c) requires an input for temperature and H_2O but produces pressure values with a SEE of only ± 150 MPa.

Clinopyroxene composition thermobarometry

To act as an independent test of pressure and temperature estimates derived from clinopyroxene-melt thermobarometers,

the clinopyroxene thermometer of Nimis and Taylor (2000) and clinopyroxene barometer of Nimis (1995) can be applied. However, due to the reported errors produced by these models when applied to hydrous systems, the recalibrated forms of these models were used (Putirka 2008, equation 32d/32b). The recalibrated barometer comes at the expense of an additional H_2O_{melt} input and is referred to in this study as P08-32d/b. The SEE of these models are ± 87 °C and ± 260 MPa, respectively.

Amphibole thermobarometry/hygrometry

The presence of amphibole-bearing, cumulate xenoliths (Group 2) allows application of the amphibole thermobarometer and hygrometer of Ridolfi et al. (2010), a group of formulations that are empirically calibrated for calc-alkaline volcanoes in island arcs. This model is referred to as Rd10 in this study and requires only compositional data of calcic amphibole to produce estimates of P–T conditions, H_2O_{melt} and fO_2 (SEE = ± 54 MPa, ± 57 °C, ± 0.41 wt.% H_2O and ± 0.41 log units fO_2), rendering it highly versatile.

Results

Petrography of the 2007–2008 lava dome

The 2007–2008 dome lava (Supplementary material 1) consists of highly porphyritic basaltic andesite with 50–55 vol.% of complexly zoned plagioclase (30–35 vol.%), orthopyroxene (5–10 vol.%) and clinopyroxene (5–10 vol.%) phenocrysts, alongside Ti-magnetite (~5 vol.%) micro-phenocrysts and trace amounts of apatite. These are set in a partly microcrystalline groundmass (45–50 vol.%) of similar mineralogy, with minor rhyolitic glass present (≤ 5 vol.%). Glomerocrysts typically display similar mineral assemblages, although they are generally dominated by clinopyroxene, orthopyroxene or plagioclase. Magmatic xenoliths are meta-basaltic and cumulate (e.g. gabbroic) in nature but exhibit mineral assemblages similar to the 2007–2008 dome lava. The basaltic xenoliths, however, have higher olivine contents, while the gabbroic xenoliths include both olivine and amphibole. Crustal xenoliths within the 2007–2008 dome lava are of calc-silicate and volcanoclastic hornfels nature.

Plagioclase is present within the basaltic andesite as phenocrysts (typically 0.5–2.0 mm), micro-phenocrysts (typically 0.01–0.50 mm), inclusions within glomerocrysts, inclusions within pyroxene phenocrysts and groundmass microlites (< 0.01 mm) (Fig. 2). Crystals are predominantly euhedral to subhedral, but rounded crystal corners and partially embayed crystal faces are frequently observed and are dominant within the micro-phenocryst population. Inclusions of glass, clinopyroxene, Ti-magnetite and small quantities of apatite (< 100 μm) are often present in larger

plagioclase crystals. Phenocrysts typically display complex zoning patterns, including oscillatory zonation, sieve textures (discrete zones exhibiting a high abundance of elliptical, partially crystalline melt inclusions) and resorption surfaces. Micro-phenocrysts are primarily unzoned but mostly display heavily resorbed, ragged crystal edges. Plagioclase crystals in glomerocrysts are also predominantly unzoned (0.05–0.5 mm) and, in some cases, represent the dominant mineral phase within the crystal clusters, but can be almost entirely absent in others (Fig. 2a). Based upon crystal sizes and petrographic criteria, the phenocrysts and micro-phenocrysts are divided into three groups; Type 1 (sieve textures and oscillatory zoning), Type 2 (oscillatory zoning only) and Type 3 (unzoned and resorbed). The key features associated with each of the main groups are shown in Fig. 3. Type 1 plagioclase crystals are characterised by a complex pattern of oscillatory zoning, sieve-textured zones and resorption surfaces and account for ~10 % of the plagioclase population (Figs. 2b, 3). Oscillatory zonation exists both as regions of clearly defined, laterally continuous growth layers and as poorly defined regions exhibiting laterally discontinuous and embayed growth layers. Discrete growth layers range from ~5 to ~40 μm in thickness, although this variation may be affected by cutting orientation. Sieve-textured zones are well defined with distinct boundaries that commonly cross twin planes. The constituent inclusions are almost exclusively partially crystallised glass but are mineral inclusions occasionally. Petrographically, cores are often distinctive, with many Type 1 crystals exhibiting a clear to sieve-textured core (Figs. 2c, 3). Sieve-textured cores are commonly surrounded by an unzoned rim, occasionally exhibiting oscillatory zoning at the outermost crystal surface. The core-rim boundaries are well defined and often display rounded and embayed edges. Type 2 plagioclase crystals are characterised by exclusive oscillatory zoning, with no sieve-textured zones present. They represent ~10 % of the plagioclase crystals present. Two common sub-types exist, the first shows oscillatory zoning that becomes narrower from core to rim (Figs. 2d, 3). Here, individual growth zones are often undulating but laterally continuous, with thicknesses ranging from < 5 to 60 μm . The second sub-type exhibits un-zoned cores and oscillatory zoned mantles and rims (Figs. 2e, 3). The core-rim boundaries are often poorly defined, although in some instances, clearly distinguishable cores are present, which are the bounded by resorption surfaces that truncate previous growth layers. Type 3 plagioclase crystals comprise small and heavily resorbed crystals (Figs. 2f, g, 3) that represent ~80 % of the plagioclase crystal population. Small melt inclusions are frequently present, but show no preferred orientation and are not restricted to individual growth layers or zones. All of the Type 3 plagioclase crystals display heavily

resorbed rims, with many being almost entirely dissolved. In some instances, patchy zoning is observed, although this is uncommon.

Orthopyroxene is present in the 2007–2008 lava dome as phenocrysts, micro-phenocrysts, groundmass microlites and, rarely, as inclusions within glomerocrysts. The largest crystal sizes display euhedral and subhedral crystal forms

and often have oxide inclusions (Ti-magnetite). The smaller crystals display predominantly subhedral and anhedral forms. When orthopyroxene is found as a constituent of glomerocrysts, it is associated primarily with Ti-magnetite but also occasionally with plagioclase. The glomerocryst orthopyroxene crystals are generally anhedral, may account for >50 % of the materials that make up

Fig. 2 Representative photomicrographs of textures observed within the Kelut 2007–2008 dome lava
a Plagioclase-dominated glomerocryst. **b** Type 1 plagioclase crystal. (I) Unzoned and resorbed crystal core. (II) Coarse sieve-textured zone. (III) Undulating oscillatory zoning. (IV) Well-defined, fine sieve-textured zone. (V) Oscillatory zoned rim **c** Type 1 plagioclase crystal. (I) ‘Spongy’ sieve-textured crystal core. (II) Unzoned rim grading into (III) oscillatory zonation. **d** Type 2 plagioclase crystal. (I) Two distinctive crystal cores, each displaying a darker interior and lighter rim (II) Continuous, undulating oscillatory zoning of varying thickness. **e** Type 2 plagioclase crystal. (I) Heavily resorbed, unzoned crystal core. (II) Oscillatory zonation. **f** Unzoned, heavily resorbed Type 3 plagioclase crystal (image centre). **g** Various sizes of unzoned, heavily resorbed Type 3 plagioclase crystals. **h** Heavily resorbed orthopyroxene crystals with clinopyroxene overgrowths and multiple Ti-magnetite inclusions

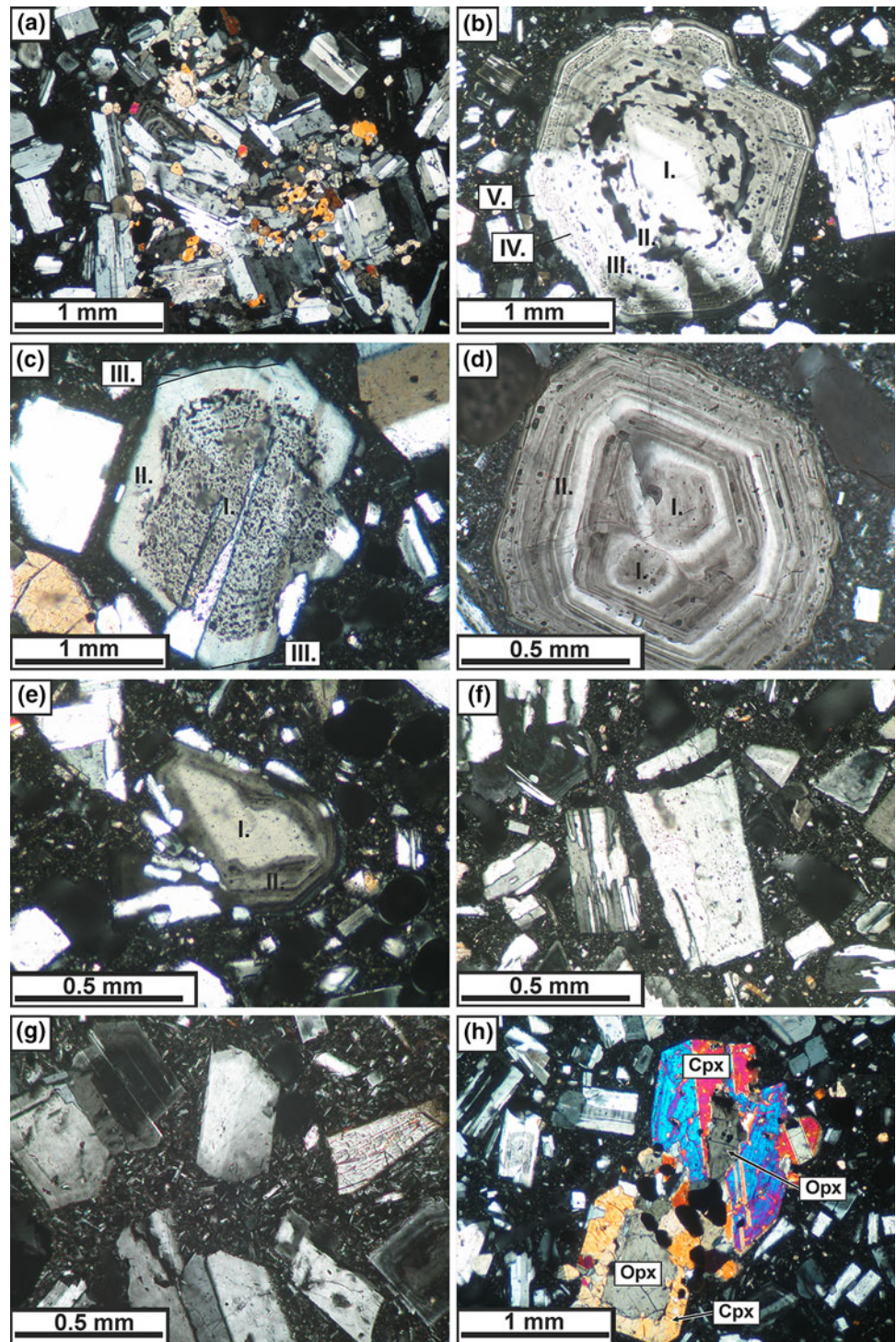
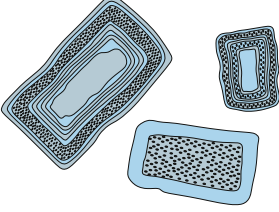
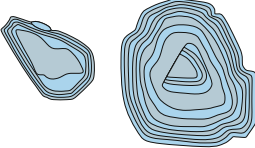

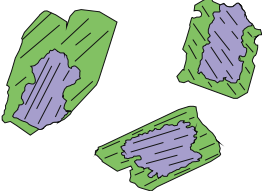
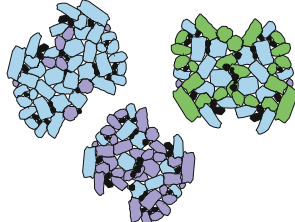


Fig. 3 Schematic summary of textures and zoning patterns of phenocrysts and micro-phenocrysts within the Kelut 2007–2008 lava dome

Mineral	Textures	Petrography
Plagioclase (type 1)		Discrete, fine sieve-texture and oscillatory zoning Occasional sieve-texture or clear cores Average length = 0.54 mm
Plagioclase (type 2)		Oscillatory zoning only Occasional resorbed cores, exhibiting truncated zoning Average length = 0.32 mm
Plagioclase (type 3)		Heavily resorbed micro-phenocryst population Average length = 0.09 mm
Pyroxene		Mantled pyroxenes Heavily resorbed orthopyroxene cores surrounded by clinopyroxene
Plagioclase, Pyroxene and Ti-magnetite		Glomerocrysts, with three end-members: Plagioclase-dominated Orthopyroxene-dominated Clinopyroxene-dominated

a single cluster and show at least partially equilibrated crystal junctions, as described by Elliott et al. (1997) and Holness (2005).

Clinopyroxene is also present as phenocrysts, micro-phenocrysts, groundmass microlites and as inclusions within glomerocrysts. Clinopyroxene crystals are predominantly euhedral to subhedral, have a large size range and tend to become more anhedral with decreasing size. Crystals often exhibit partially resorbed crystal faces and, occasionally, oscillatory zonation in the outermost rims. Inclusions of Ti-magnetite are common in clinopyroxene, reaching sizes of up to 300 μm . The glomerocryst clinopyroxene is associated primarily with Ti-magnetite and plagioclase, usually accounting for >50 % of the crystals that make up a given cluster. Examples of clinopyroxene rims enclosing heavily resorbed and fractured orthopyroxene are here referred to as ‘mantled pyroxenes’. Such

features have been observed at other Indonesian volcanoes, for example, Merapi (Gertisser and Keller 2003), Rinjani (Foden 1982), Gede (Handley et al. 2010) and Slamet (Reubi et al. 2002). Clinopyroxene rims are usually $\sim 150 \mu\text{m}$ in thickness, but reach 300 μm in some instances. Clinopyroxene rims do not always enclose the cores entirely, but mantle a single growth twin or a single crystal face (Fig. 2h).

Ti-magnetite (as well as trace amounts of apatite) are present as a micro-phenocryst population and as inclusions predominantly within pyroxene phenocrysts. Both phases exhibit euhedral to anhedral crystal forms that rarely exceed 400 μm in size and often occur in close proximity to pyroxenes and glomerocrysts.

A variety of xenoliths are present within the 2007–2008 dome lava, some of igneous origin, others meta-volcanic or calc-silicate in nature (Supplementary material

1). Considerable variation in crystal sizes (0.02–20 mm), textures and mineralogy allows the distinction of three groups: (Meta-) igneous xenoliths (Group 1) are typically <10 cm across and are defined by fine grain sizes (typically <0.05 mm). The main mineral phases are plagioclase, clinopyroxene and Ti-magnetite. They often exhibit well-developed hornfels textures or highly rounded crystals and large, optically continuous clinopyroxene crystals filled with small, lobate plagioclase and Ti-magnetite inclusions. Crystals are almost exclusively unzoned. Individual xenoliths generally comprise a dominantly fine-grained core, surrounded by a rim of significantly larger clinopyroxene and plagioclase crystals (0.5–2.0 mm), the latter occasionally exhibiting complex oscillatory and sieve texture zonation, similar to previously described 2007–2008 dome lava, Type 1 and Type 2 plagioclase crystals. Cumulate xenoliths (Group 2) are coarse-grained and can reach sizes of ~10 cm across. They are characterised by cumulus textures (low groundmass %, crystal framework with interstitial phases) and display an assemblage of plagioclase, poikilitic clinopyroxene, orthopyroxene, poikilitic amphibole, olivine and Fe–Ti oxides. Plagioclase crystals vary in size from 0.1 to 20 mm, are usually unzoned and, alongside amphibole, represent the cumulus phase. Olivine exists dominantly as anhedral inclusions (<0.5 mm) within amphibole megacrysts (<0.5–20 mm). Relative proportions and the degree of breakdown of amphibole vary considerably between samples, ranging effectively between two end-members; the first containing large (2–20 mm), unzoned amphibole crystals with distinctive breakdown rims, the second containing small, ragged crystals (<0.5 mm) that exhibit more advanced breakdown rims. Orthopyroxene and clinopyroxene represent interstitial phases. Meta-sedimentary xenoliths (Group 3) are both meta-volcaniclastic rocks and calc-silicates, typically <10 cm across and display mineral assemblages of plagioclase, clinopyroxene, orthopyroxene and Fe–Ti oxides, and wollastonite, clinopyroxene and quartz, respectively. Characteristics such as rounded grains, lack of compositional zonation and the presence of fluid pathways indicate a sedimentary origin and contact metamorphism during entrainment within a melt. Individual crystals rarely exceed 4 mm.

Mineral chemistry

All mineral compositional data are provided in Supplementary material 2. The plagioclase population of the 2007–2008 lava dome exhibits a compositional range of An_{47–94} (Fig. 4a). Type 1 and Type 2 crystal cores are generally calcic (An_{74–92}), and the typical variation from core to rim is 10–20 mol.%. Individual growth zones frequently vary in thickness and display undulating

boundaries, but compositional changes across these boundaries are commonly less than 5 mol.%, with entire crystals defined by rapidly fluctuating An up to 30 mol.% variability (Supplementary material 3). Individual growth layers that are An depleted but enriched in Fe and Mg can be seen occasionally. Compositionally, Type 3 plagioclase crystals are distinct from both Type 1 and Type 2 crystals by their generally more calcic compositions and their lack of chemical zonation. Plagioclase crystals within meta-basaltic xenoliths (Group 1) are not compositionally zoned, but together span a considerable compositional range (An_{29–91}) (Fig. 4a). Plagioclase crystals found within cumulate xenoliths (Group 2) also lack compositional zonation, but as a group, they span a significantly smaller compositional range than Group 1 xenolith plagioclase (An_{64–96}) (Fig. 4a).

Orthopyroxene crystals in the 2007–2008 lava dome are exclusively enstatite (according to the classification scheme of Morimoto et al. 1988). They show relatively uniform compositions (En_{64–72}, Fs_{24–32}, Wo_{2–4}) and are unzoned. Dome clinopyroxenes are classified as diopside to augite (En_{40–48}, Fs_{14–19}, Wo_{34–46}) (Fig. 4b). Clinopyroxene from meta-basaltic (Group 1) xenoliths ranges from augite to diopside/hedenbergite (En_{1–42}, Fs_{14–50}, Wo_{42–50}) and exhibit a greater variety of compositions than those of the 2007–2008 dome lavas. Clinopyroxene from cumulate xenoliths (Group 2) extends to higher Ca contents than both the dome clinopyroxenes and the meta-basaltic (Group 1) clinopyroxenes, and classifies as augite to diopside (En_{35–43}, Fs_{9–17}, Wo_{42–50}).

Ti-magnetite micro-phenocrysts and amphibole megacrysts exhibit very limited geochemical variation, with Ti-magnetite compositions that range from Usp_{16–34} (Fig. 4c) and amphiboles that are uniformly calcic, and can be classified as magnesiohastingsite using the scheme of Leake et al. (1997) (Fig. 4d). Titanium contents of Ti-magnetites are typically between 8.1 and 11.1 wt.%. Aluminium contents of amphiboles range from 13.8 to 14.4 wt.%.

Major and trace element geochemistry

Major and trace element data for the 2007–2008 lava dome and cumulate xenolith (Group 2) samples are given in Tables 1 and 2. The 2007–2008 dome lava samples are plotted in Harker-type variation diagrams and classified alongside new and published data for the 1990 eruption and unspecified pre-1990 eruptions (Bourdier et al. 1997; van Bergen et al. 2000; this study) (Supplementary material 4), in addition to the K₂O versus SiO₂ scheme of Le Maitre (1989) (Fig. 5). Analyses for groundmass glass and plagioclase-hosted melt inclusions for the 2007–2008 dome are also shown (Table 3).

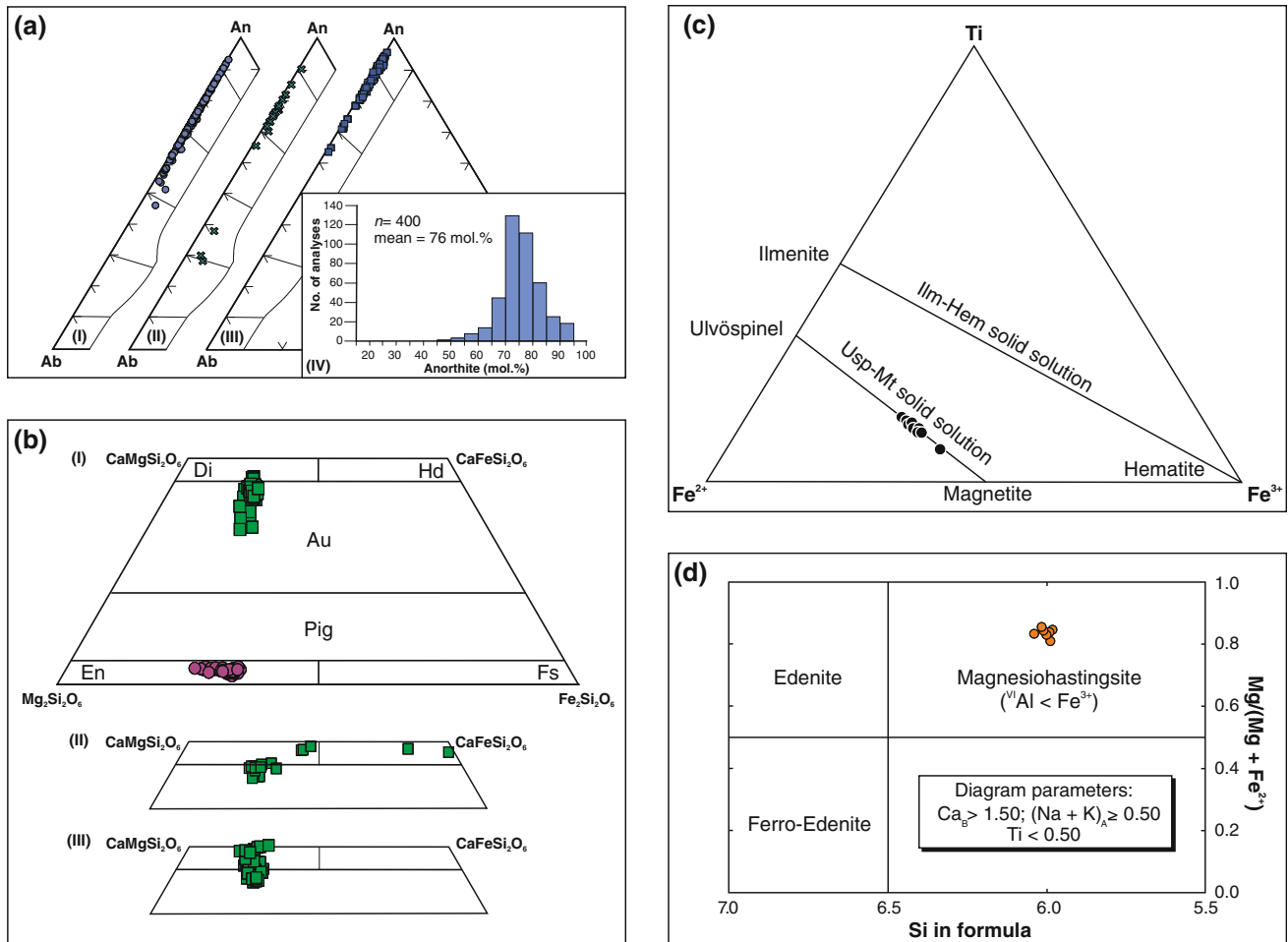


Fig. 4 **a** Feldspar ternary classification diagrams for (I) 2007–2008 lava dome plagioclase, (II) Meta-basaltic xenolith (Group 1) plagioclase and (III) Cumulate xenolith (Group 2) plagioclase. (IV) Histogram of 2007–2008 dome lava plagioclase anorthite contents. **b** Pyroxene quadrilateral classification scheme of Morimoto et al. (1988) for (I) 2007–2008 lava dome orthopyroxene and clinopyroxene, (II) Meta-basaltic xenolith (Group 1) clinopyroxene and (III)

Cumulate xenolith (Group 2) clinopyroxene **c** Ternary classification of analysed oxide minerals in the 2007–2008 lava dome **d** Cumulate xenolith (Group 2) amphibole analyses plotted in the classification scheme of Leake et al. (1997). *An* anorthite, *Ab* albite, *En* enstatite, *Fs* ferrosilite, *Pig* pigeonite, *Au* augite, *Di* diopside, *Hd* hedenbergite, *Usp* ulvöspinel, *Ilm* ilmenite, *Hem* hematite, *Mt* magnetite

The Kelut 2007–2008 lava dome has a similar composition and shows the same limited geochemical variation as the 1990 samples, straddling the boundary between the low- and medium-K basaltic andesite field (Fig. 5). Pre-1990 samples appear to deviate somewhat from the 1990 and 2007–2008 samples in major element geochemistry, although this potential variation is based upon only two analyses. Typical whole rock SiO₂ contents range from 54 to 56 wt.% (Table 1). Whole rock, melt inclusion and groundmass glasses each form discrete data fields which, for Al₂O₃, Fe₂O₃^{*}, MgO and CaO, show an overall negative correlation with increasing silica. Data for TiO₂ display uniform values (~0.7 wt.%) with increasing silica. Data for P₂O₅ and K₂O show pseudo-positive correlations, whilst whole rock and groundmass Na₂O contents are relatively uniform (~3 wt.%), with melt inclusion data

deviating notably from this range (3.5–5.5 wt.%). Cumulate xenoliths (Group 2) are generally gabbroic and show some geochemical variation from 44 to 48 wt.% SiO₂, 19 to 28 wt.% Al₂O₃, 3 to 7 wt.% MgO and 5 to 11 wt.% Fe₂O₃^{*} (Table 1).

Plagioclase-hosted melt inclusions within the 2007–2008 dome lava have SiO₂ contents between ~70 and 73 wt.% and are classified as rhyolite (Fig. 5). Chlorine concentrations range from 2,000 to 4,000 ppm, whereas sulphur contents are typically below the electron microprobe detection limit (~115 ppm). Contents of Al₂O₃ (~9 to 12 wt.%), Fe₂O₃^{*} (~5 to 7 wt.%), MgO (~0.5 to 2 wt.%) and CaO (~1.5 to 3 wt.%) are significantly lower than whole rock samples, whereas the alkalis are significantly higher (Na₂O ~3 to 6 wt.%, K₂O ~2 to 4 wt.%; Table 3). Groundmass glass analyses show similar

Table 1 Major element (wt.%) compositions of the 2007–2008 lava dome and associated Group 2 xenoliths as well as scoria and pumice clasts from the 1990 eruption and unspecified pre-1990 eruptions

Eruption/stage	2007/08	2007/08	2007/08	2007/08	2007/08	2007/08	2007/08	2007/08	1990	1990	1990	1990	1990	1990	1990	1990	1990	Pre-1990	Pre-1990
Sample	KLT-K2	KLT-71a	KLT-K3	KLT-A	K-A1	K-PX2	K-PX3	K-PX7	KLT-901	KLT-902	KLT-903	KLT-904	5	4	3	2	1		
Sample type	L	L	L	L	L	G2x	G2x	G2x	P	P	P	P	S	S	S	P	P	P	P
SiO ₂	54.86	54.45	54.10	54.04	55.00	47.52	44.53	46.49	53.93	54.48	54.30	54.26	55.05	55.24	56.06	56.15	55.19		
TiO ₂	0.70	0.75	0.68	0.73	0.65	0.72	0.39	0.73	0.67	0.63	0.67	0.73	0.62	0.62	0.58	0.57	0.58		
Al ₂ O ₃	18.83	18.57	18.60	18.62	18.84	18.69	28.13	19.45	18.56	18.49	18.59	18.78	18.50	18.70	18.48	18.28	18.20		
Fe ₂ O ₃ *	8.86	8.90	8.58	8.77	8.96	11.94	5.93	11.58	9.06	8.76	8.81	8.66	8.84	8.71	8.23	6.46	7.51		
MnO	0.21	0.21	0.20	0.20	0.20	0.26	0.10	0.25	0.21	0.21	0.21	0.20	0.21	0.20	0.20	0.16	0.17		
MgO	3.91	4.02	3.85	3.94	3.80	6.75	3.01	6.94	3.96	3.87	3.91	3.93	3.74	3.50	3.94	3.43	3.85		
CaO	9.16	9.15	9.08	9.19	9.10	13.07	15.91	13.49	9.16	9.01	9.14	9.29	9.20	9.09	9.15	8.48	8.86		
Na ₂ O	3.00	2.97	2.99	2.95	2.94	1.37	1.12	1.25	2.92	2.99	2.96	2.96	3.05	3.11	3.30	2.39	2.42		
K ₂ O	0.72	0.72	0.73	0.72	0.71	0.15	0.07	0.09	0.69	0.74	0.74	0.72	0.79	0.83	0.53	0.59	0.57		
P ₂ O ₅	0.14	0.13	0.14	0.14	0.13	0.03	0.01	0.02	0.13	0.14	0.13	0.14	0.00	0.00	0.08	0.07	0.08		
LOI	<0.10	<0.10	0.10	<0.10	–	–	–	–	<0.10	<0.10	<0.10	<0.10	–	–	–	–	–		
Total	100.39	99.87	98.95	99.30	100.33	100.48	99.20	100.27	99.29	99.32	99.46	99.67	100.00	100.00	100.55	96.58	97.43		

Samples 1–3 are from Bernard (unpubl. data); samples 4–5 are from Bourdier et al. (1997). Sample type: L lava, G2x Group 2 xenolith, P pumice, S scoria
 * Total iron given as Fe₂O₃

Table 2 Trace element (ppm) compositions of the 2007–2008 lava dome and the 1990 eruption, determined by ICP-MS

Eruption/stage	2007/08	2007/08	2007/08	2007/08	1990	1990	1990	1990
Sample	KLT-K2	KLT-71a	KLT-K3	KLT-A	KLT-901	KLT-902	KLT-903	KLT-904
Sample type	L	L	L	L	P	P	P	P
Cs	1.0	1.0	0.9	0.9	0.9	1.0	1.0	0.9
Rb	13.5	13.3	13.1	13.0	12.8	13.7	12.9	12.6
Ba	499	501	504	505	466	509	480	488
Sr	631.9	623.0	620.6	621.6	618.4	608.2	608.1	615.3
Be	<1	<1	<1	<1	1	<1	<1	<1
Mo	0.2	0.3	<0.1	0.2	0.2	<0.1	0.1	<0.1
Pb	0.8	0.8	1.3	1.9	2.7	0.9	0.9	0.9
Zr	46.2	45.3	43.6	45.0	43.5	46.0	43.0	43.8
Nb	1.1	1.2	1.1	1.2	1.2	1.2	1.2	1.1
Hf	1.5	1.5	1.6	1.3	1.4	1.2	1.5	1.5
Ta	<0.1	<0.1	<0.1	<0.1	<0.1	<0.1	<0.1	<0.1
Th	1.2	1.1	1.0	1.1	1.2	1.1	0.8	1.2
U	0.4	0.4	0.3	0.4	0.4	0.4	0.4	0.4
Y	16.4	16.1	15.6	15.8	14.9	15.6	15.1	15.6
Cu	28.9	33.8	21.1	26.7	35.2	53.4	30.4	49.4
Zn	24	26	9	27	26	23	22	20
Ni	3.5	3.5	1.2	3.5	4.1	3.7	2.9	4.4
Co	21.2	21.6	20.7	21.1	20.6	23.4	22.0	23.2
V	210	221	200	210	208	202	203	208
La	5.7	5.8	5.7	5.7	5.6	5.9	5.5	5.5
Ce	13.3	13.8	13.1	13.3	12.8	13.7	13.2	12.6
Pr	1.80	1.79	1.70	1.74	1.72	1.80	1.72	1.71
Nd	9.1	7.9	8.1	8.8	8.6	9.1	8.7	8.0
Sm	2.16	2.23	2.20	2.22	2.03	2.25	2.24	2.16
Eu	0.84	0.88	0.81	0.85	0.80	0.85	0.83	0.81
Gd	2.51	2.52	2.51	2.57	2.34	2.51	2.44	2.44
Tb	0.45	0.44	0.43	0.44	0.40	0.44	0.42	0.44
Dy	2.65	2.66	2.51	2.69	2.46	2.68	2.50	2.54
Ho	0.58	0.58	0.55	0.56	0.55	0.55	0.55	0.53
Er	1.72	1.71	1.78	1.75	1.58	1.64	1.71	1.71
Tm	0.27	0.27	0.26	0.27	0.25	0.27	0.25	0.26
Yb	1.75	1.76	1.74	1.76	1.66	1.72	1.68	1.71
Lu	0.28	0.27	0.27	0.28	0.25	0.28	0.26	0.27
Ga	16.4	15.9	15.5	15.8	15.0	15.6	15.7	15.2

Sample type: *L* lava, *P* pumice

behaviour and plot as rhyolite, with SiO₂ contents between 73 and 76 wt.%, and low Fe₂O₃^{*} (~2 to 4 wt.%) and MgO (~0.25 to 0.55 wt.%) contents (Fig. 5, Supplementary material 4, Table 3). Chlorine concentrations of ground-mass glass range between 1,400 and 2,400 ppm, whereas sulphur concentrations are typically below the detection limit (see above).

Chondrite-normalised REE patterns for the 2007–2008 dome lava show minor LREE enrichment (up to ~25 × relative to chondrite) relative to HREE (~10 × relative to chondrite) (Supplementary material 5) with constant La_N/Yb_N ratios of 3.2–3.3, and unfractionated MREE to HREE, with Gd_N/Sm_N ratios of ~1.4. A

multi-element diagram is presented in Supplementary material 5, where the data are normalised against N-MORB (Sun and McDonough 1989). The Kelut dome lava exhibits enrichment of large-ion lithophile elements (LILE) Rb, Ba, K and Sr, in addition to U, Th and Pb, relative to typical N-MORB concentrations. In contrast, Nb and Ti show pronounced troughs, whereas MREE and HREE are all depleted relative to N-MORB values. All LREE exhibit up to 2.3 × enrichment relative to N-MORB, with the exception of Eu and Sm, which are mildly depleted. Trace element patterns of the 1990 samples are almost identical to those of the 2007–2008 dome lava (Table 2, Supplementary material 5). A notable feature of the Kelut rocks,

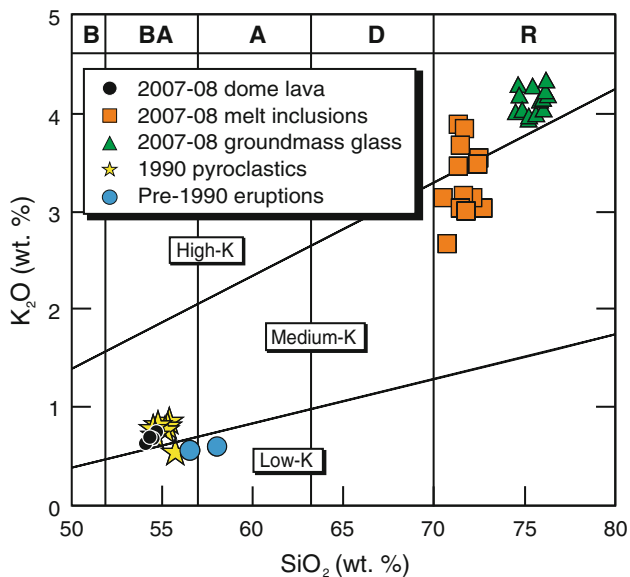


Fig. 5 K_2O versus SiO_2 diagram (Le Maitre 1989) displaying whole rock analyses of the 2007–2008 dome lava, alongside the 1990 eruption and unspecified pre-1990 eruptions (Bourdier et al. 1997; van Bergen et al. 2000). Also plotted, plagioclase-hosted melt inclusions and groundmass glass analyses from the 2007–2008 lava dome. All data recalculated to 100 % (on a volatile-free basis). B basalt, BA basaltic andesite, A andesite, D dacite, R rhyolite

compared to calc-alkaline basaltic andesites from other Sunda arc volcanoes (e.g. Merapi in Central Java; c.f. Gertisser and Keller 2003), is the only minor LREE enrichment in chondrite-normalised REE diagrams (Supplementary material 5).

Oxygen isotopes

Plagioclase crystals extracted from the 2007–2008 dome lava have $\delta^{18}O$ values between 6.5 and 7.6 ‰ ($n = 3$), whilst pyroxenes yield values of 5.4–6.7 ‰ ($n = 5$) (Table 4). The whole rock $\delta^{18}O$ value of the dome lava is 7.6 ‰, which is elevated relative to I-MORB. The whole rock $\delta^{18}O$ values of meta-basaltic (Group 1) and calc-silicate (Group 3) xenoliths are 6.2 and 10.3 ‰, respectively. These xenolith values are similar to those of xenoliths found in recently extruded lavas from Merapi volcano in Central Java, Indonesia (Table 4; Gertisser and Keller 2003; Troll et al. 2013). The new $\delta^{18}O$ values described for Kelut are similar to those of other Javanese volcanoes that lie either within or marginally higher than the typical range of mantle-derived magmas such as MORB (Harmon and Hoefs 1995) and I-MORB (Ito et al. 1987). Examples of Javanese volcanoes where $\delta^{18}O$ values are available include: Galunggung (whole rock 5.8–6.4 ‰, Gerbe et al. 1992; 5.6 to 6.0 in plagioclase and 5.3–5.6 in pyroxene, Harmon and Gerbe 1992); Merapi (whole rock 5.6–8.3 ‰, Gertisser and Keller 2003; Troll et al. 2013);

Ringgit–Beser (whole rock 6.1–7.1 ‰, Edwards et al. 1994); Gede (5.5–6.0 ‰ in clinopyroxene and 6.0 ‰ in plagioclase, Handley et al. 2010); Salak (5.2–5.4 ‰ in clinopyroxene and ~6.0 ‰ in plagioclase, Handley et al. 2008); Ijen (5.4–5.6 ‰ in clinopyroxene and 6.1 ‰ in plagioclase, Handley et al. 2007). Bulk-rock and mineral $\delta^{18}O$ values are not exactly equivalent and do not represent directly magma $\delta^{18}O$ values. This is due to the effects of alteration in the former and mineral–magma fractionation in the latter, as discussed below (e.g. Hoefs 2005).

Crystal size distribution data

Calculated CSD plots for all mineral phases in the 2007–2008 dome lava (Fig. 6) exhibit kinked or curved profiles, allowing each to be broken down into two or more individual segments. Calculated input parameters and results are shown in Table 5.

The CSD plots for plagioclase all lie within a distinct band and range from a smooth, concave-upward slope to a moderately kinked, straight slope (Fig. 6a, f). Each curve can be divided into two distinctive populations, defined by size (<0.25 and >0.25 mm), slope value (–11.661 to –15.894 mm and –4.089 to –5.817 mm) and intercept (6.630–7.798 mm^{–4} and 4.341–5.669 mm^{–4}). Volumetric phase proportions range from 25.6 to 33.9 vol.%. Characteristic length values, calculated using the formula ‘Characteristic length = –1/Slope’ (Marsh 1988), range from 0.063 to 0.086 mm for the smaller populations and 0.172 to 0.245 mm for the larger populations. The CSD plots created using plagioclase groundmass microlites show straight-line profiles (Fig. 6b, g, h). A downturn in the smallest crystal sizes of both samples is considered to represent a left-hand truncation effect resulting from the difficulty in resolving the smallest crystal population. Slope values range from –125.05 to 139.93 mm. Slope intercepts range from 19.497 to 19.697 mm^{–4}. Calculated characteristic lengths range from 0.007 to 0.008 mm.

Orthopyroxene CSDs show smooth concave-upward slopes that become strongly kinked at crystal sizes <0.15 mm (Fig. 6c, f). A pronounced downturn of the slope in the smallest crystal sizes of sample Kelut-A is considered to be a left-hand truncation effect. Both CSDs can be divided into two slopes (<0.20 and >0.20 mm). Slope values range from –20.273 to –26.519 mm and –2.524 to –6.430 mm. Slope intercepts range from 6.414 to 7.546 mm^{–4} and 1.913 to 3.540 mm^{–4}. Volumetric phase proportions range from 3.1 to 7.5 vol.%. Calculated characteristic lengths range from 0.038 to 0.049 mm for the smaller populations and 0.156 to 0.396 mm for the larger populations.

The CSD plots for clinopyroxene exhibit predominantly kinked patterns that can be divided into two distinct slopes

Table 3 Major element and volatile concentrations of 2007–2008 lava dome plagioclase-hosted melt inclusions and groundmass glass

Sample Analysis	KPX-6B A02	KPX-6B B01	KPX-6B B03	KPX-6B B05	KPX-6B B06	KPX-6B B07	KPX-6B C01	KPX-6B D01	KPX-6B F01	KPX-6B G01	KPX-6B H01	KPX-6B H03	KPX-6B I01	
Plagioclase-hosted melt inclusions														
SiO ₂	70.18	70.49	69.05	70.42	70.99	70.59	71.13	70.55	71.92	69.76	71.69	72.53	70.98	
TiO ₂	0.96	0.75	0.72	0.69	0.69	0.70	1.01	0.67	0.78	0.79	0.63	0.69	0.85	
Al ₂ O ₃	9.63	9.95	11.35	10.84	11.80	11.12	9.34	10.86	10.70	10.34	11.37	10.76	10.48	
FeO*	5.98	5.89	5.30	4.96	4.55	4.77	5.83	5.60	5.69	5.93	5.23	5.56	5.75	
MnO	0.25	0.23	0.18	0.18	0.17	0.17	0.25	0.23	0.18	0.23	0.20	0.22	0.19	
MgO	1.67	1.74	1.10	1.24	1.11	1.25	1.65	1.46	0.86	1.70	1.14	1.25	1.53	
CaO	2.21	2.45	2.09	2.34	1.83	1.89	2.16	2.04	1.66	2.81	1.80	1.93	2.08	
Na ₂ O	3.93	4.01	5.09	4.60	4.32	4.04	3.83	3.92	3.82	3.96	3.58	3.72	3.53	
K ₂ O	2.98	3.03	2.61	3.12	3.88	3.79	3.09	3.43	3.52	3.10	3.45	3.03	3.66	
P ₂ O ₅	0.49	0.37	0.21	0.25	0.27	0.22	0.39	0.22	0.28	0.37	0.17	0.19	0.37	
Total	98.29	98.90	97.71	98.64	99.60	98.54	98.68	98.98	99.41	98.99	99.26	99.88	99.42	
Cl (ppm)	3,660	3,411	2,465	2,014	2,374	2,533	3,970	2,920	3,467	3,403	2,335	2,421	2,665	
S (ppm)	b.d.	b.d.	b.d.	b.d.	b.d.	b.d.	184	154	b.d.	128	b.d.	b.d.	b.d.	
Sample Analysis	K-1 A01	K-1 A02	K-1 B01	K-1 B02	K-1 C02	K-1 C03	K-1 C04	K-1 C06	K-1 C07	K-1 C07b	K-1 C07c	K-1 C07d	K-1 C07e	K-1 C07f
Groundmass glass														
SiO ₂	74.63	73.97	76.05	75.77	74.87	74.71	75.35	74.73	75.54	73.74	75.66	75.46	75.57	75.95
TiO ₂	0.67	0.74	0.72	0.66	0.67	0.69	0.71	0.62	0.63	0.71	0.63	1.02	0.82	0.62
Al ₂ O ₃	12.01	12.01	11.75	11.47	11.75	11.83	11.56	11.79	11.80	11.51	11.36	11.97	11.88	11.88
FeO*	3.79	3.56	2.41	2.68	3.18	2.99	2.91	2.91	2.31	3.69	2.91	2.35	2.56	2.24
MnO	0.11	0.11	0.08	0.10	0.12	0.11	0.11	0.12	0.08	0.12	0.12	0.07	0.09	0.07
MgO	0.27	0.30	0.36	0.39	0.47	0.48	0.44	0.52	0.41	0.44	0.41	0.45	0.43	0.37
CaO	1.01	1.01	0.91	1.15	1.23	1.17	1.09	1.52	0.98	1.31	1.22	0.90	1.00	0.92
Na ₂ O	3.05	3.05	2.95	2.86	3.03	3.09	3.11	3.23	3.17	3.11	3.03	3.17	3.00	3.20
K ₂ O	4.27	4.16	4.35	4.28	3.94	3.94	3.97	4.03	4.13	3.98	4.06	4.27	4.15	4.18
P ₂ O ₅	0.21	0.22	0.28	0.25	0.31	0.30	0.34	0.40	0.31	0.39	0.31	0.23	0.22	0.26
Total	100.02	99.14	99.86	99.61	99.58	99.30	99.59	99.88	99.37	98.98	99.71	99.89	99.73	99.70
Cl (ppm)	n.d.	n.d.	n.d.	1,412	2,058	1,699	n.d.	2,433	n.d.	n.d.	n.d.	n.d.	n.d.	n.d.
S (ppm)	176	b.d.	b.d.	b.d.	b.d.	b.d.	b.d.	150	b.d.	b.d.	b.d.	b.d.	b.d.	b.d.

b.d. below detection limit

n.d. not determined

* Total iron given as FeO

Table 4 Oxygen isotope data for the 2007–2008 dome lava, mineral phases and xenoliths, with calculated melt values

Sample	Sample type	SiO ₂ (wt.%)	$\delta^{18}\text{O}_{w.r.}$	$\delta^{18}\text{O}_{px}$	$\delta^{18}\text{O}_{px \text{ melt}}$	$\delta^{18}\text{O}_{fsp}$	$\delta^{18}\text{O}_{fsp \text{ melt}}$
K-L-6	L	54.90		5.4	5.7	6.7	6.5
				5.7	6.0		
K-A-1	L	55.00		5.4	5.7	6.5	6.2
				5.6	5.9		
K-BA-08-1	L	54.59	7.6	6.7	7.0	7.6	7.4
K-L + XC-1	G3x	48.90		10.3			
K-L + XC-4	G1x	48.50		6.2			

Sample type: *L* lava, *G1x* Group 1 xenolith, *G3x* Group 3 xenolith. All $\delta^{18}\text{O}$ values are reported in ‰ relative to SMOW. See text for analytical error. *w.r.* whole rock, *px* pyroxene, *fsp* plagioclase feldspar. $\delta^{18}\text{O}$ (melt) has been determined using mineral-melt values of +0.2 and –0.3 ‰ for plagioclase and pyroxene, respectively (e.g. Kyser et al. 1981; Harris et al. 2005)

(Fig. 6d). However, this division does not correlate between CSDs. For example, the break of slope is located at ~ 0.28 mm in sample KLT-71a and at ~ 0.95 mm in sample Kelut-A. Slope values range from -5.464 to -13.957 mm and -1.990 to -3.374 mm. Slope intercepts range from 2.664 to 3.750 mm $^{-4}$ and 0.696 to 0.901 mm $^{-4}$. Volumetric phase proportions range from 4.2 to 6.4 vol.%. Calculated characteristic lengths range from 0.072 to 0.183 mm for the smaller populations and from 0.296 to 0.503 mm for the largest populations.

Ti-magnetite CSDs display variable profiles; sample Kelut-A is defined by a single straight slope, sample KLT-71a by two distinctive slopes (Fig. 6e, f). Slope values are -62.64 mm and -15.015 to -15.801 mm, respectively. Slope intercepts are 9.985 mm $^{-4}$ and 5.981 – 6.575 mm $^{-4}$. Volumetric phase abundances were determined as 3–5 vol.%. Calculated characteristic lengths are 0.016 mm for the smallest population and 0.063–0.067 mm for the largest population.

Magmatic intensive variables

Pre-eruptive H_2O_{melt} values

A number of thermobarometers utilised in this study require an initial estimate of pre-eruptive H_2O_{melt} , which was determined by applying the ‘difference method’ (Devine et al. 1995) to plagioclase-hosted melt inclusions. The precision of this method is considered to be ± 0.5 wt.%. Mass deficiencies range from 0.12 to 2.29 wt.% (average = 1.05 wt.%; $n = 13$; $1\sigma = 0.57$ wt.%). The average value of 1.05 wt.% was therefore used as a primary H_2O_{melt} input for plagioclase-melt models. Minimum and maximum values of 0.12 and 2.29 wt.% were used as alternative inputs for plagioclase-melt thermometry and hygrometry, to evaluate the control of the initial H_2O_{melt} value on calculated intensive variables.

Temperatures and H_2O_{melt} from plagioclase-melt models

The $K_D[\text{Ab}-\text{An}]$ test described by Putirka (2008) was applied to identify plagioclase compositions in equilibrium with the dome lava whole rock. On this basis, only compositions between An_{65-83} were found to be suitable for thermobarometry (Fig. 7a). This test also allows the determination of a maximum H_2O content. Using an H_2O input >4.5 wt.% results in temperature estimates below 1,050 °C and requires a $K_D[\text{Ab}-\text{An}]$ of 0.10 ± 0.05 . This renders the vast majority of analysed plagioclase crystals out of equilibrium with the 2007–2008 dome lava (cf. Putirka 2008). The maximum H_2O content is therefore constrained to ~ 4.5 wt.%.

Temperatures calculated with P08-24a range from 1,151 to 1,164 °C (average = 1,160 °C; $n = 303$). These values

are within ~ 15 °C of the calculated plagioclase saturation temperature of 1,168 °C. P08-25b yields H_2O_{melt} values between 1.5 and 1.9 wt.% (average = 1.8 wt.%; $n = 303$; $1\sigma = 0.09$ wt.%), considerably lower than those predicted by P05-mH, which range from 2.3 to 3.3 wt.% (average = 2.7 wt.%; $n = 303$; $1\sigma = 0.22$ wt.%), but consistent with values derived from melt inclusions. This lack of correlation, alongside P05-mHs’ known tendency to overestimate H_2O_{melt} values, suggests that the results of P08-25b are the more reliable ones and are thus applied for further thermobarometric calculations.

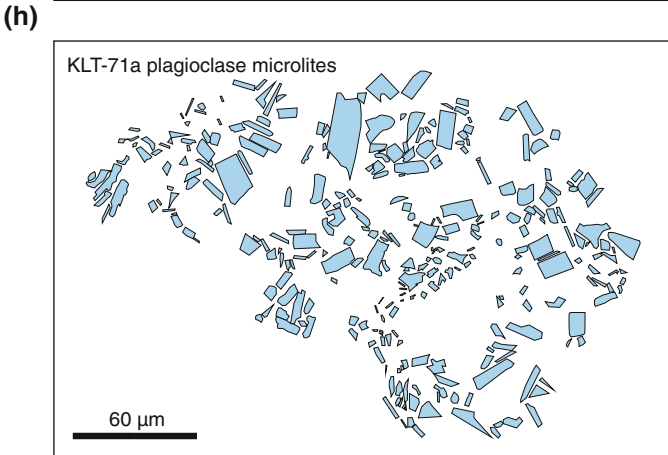
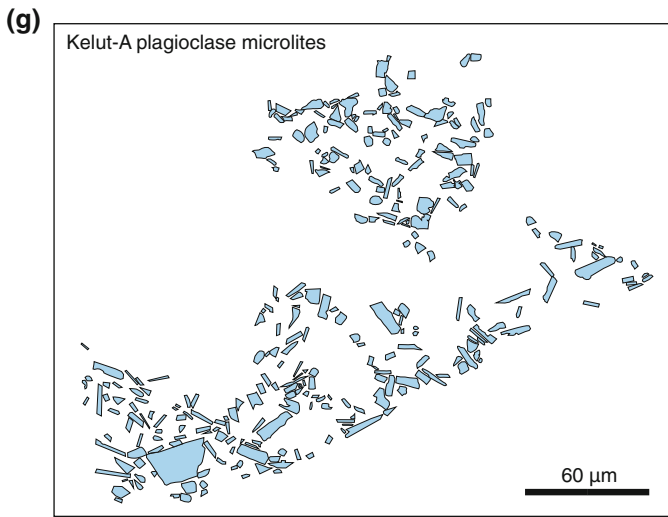
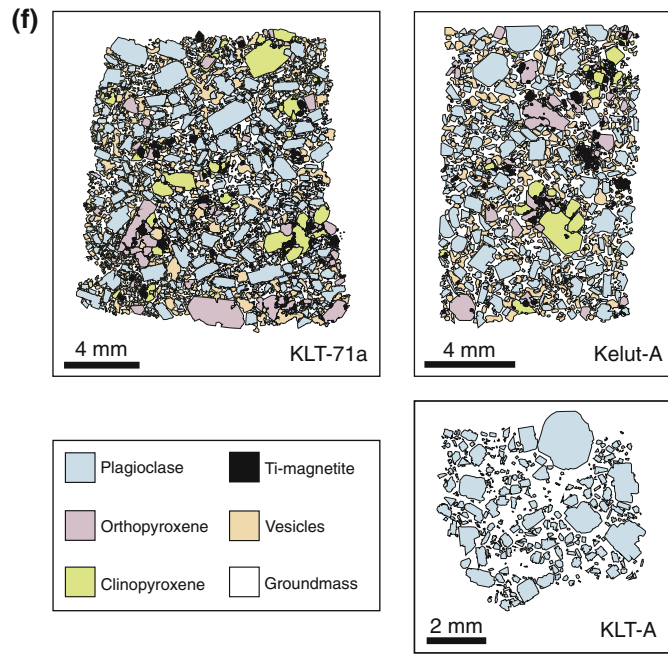
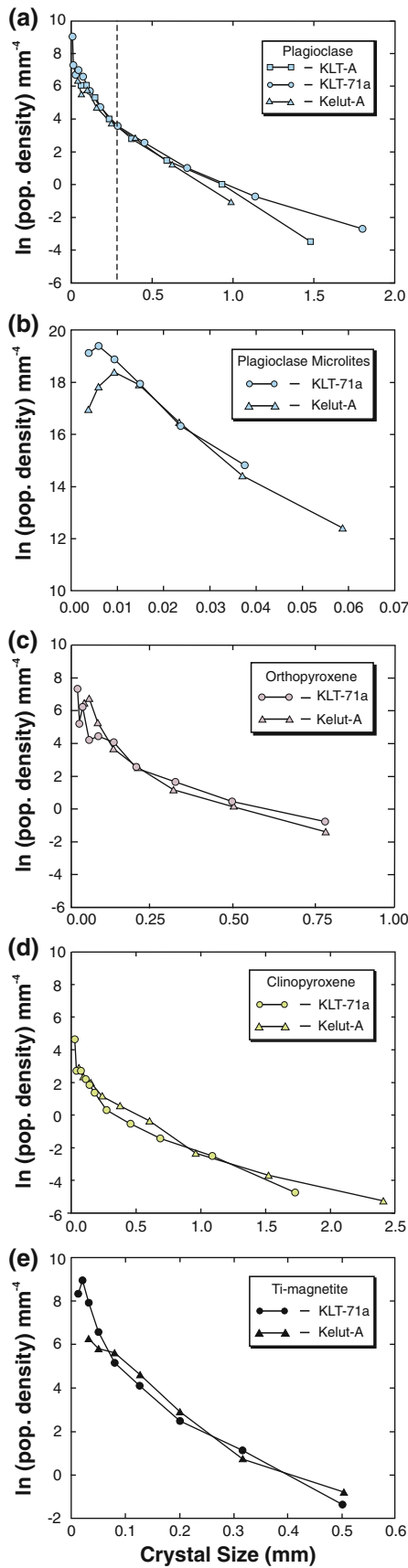
Alternative H_2O_{melt} values of 0.12 and 2.29 wt.% produce average temperature values of 1,195 °C (based upon minimum $H_2O_{\text{melt}} = 0.12$ wt.%) and 1,115 °C (based upon maximum $H_2O_{\text{melt}} = 2.29$ wt.%). The same secondary inputs produce H_2O_{melt} estimates of 0.9 and 2.6 wt.%, respectively. These H_2O_{melt} values were used as secondary inputs for clinopyroxene-melt thermobarometry.

Pressures and temperatures from clinopyroxene-melt models

To select a suitable whole rock composition for thermobarometry with clinopyroxene phenocrysts, the $K_D[\text{Fe}-\text{Mg}]$ values between clinopyroxene (rims and cores undifferentiated) and four potential melt compositions were tested (2007–2008 dome lava whole rock, cumulate xenolith (Group 2) whole rock, groundmass glass, plagioclase-hosted melt inclusion). The host rock produced values that were closest to the ideal $K_D[\text{Fe}-\text{Mg}]$ of 0.28 (Putirka 2008) and were therefore selected as the melt composition with which the majority of the clinopyroxenes had equilibrated. As an additional test, the predicted mineral components of hedenbergite and diopside were plotted against the observed components, as recommended by Putirka (2008) and Mollo et al. 2010). The majority of the clinopyroxene analyses plotted within 10 % of the one-to-one line, which suggests that they are suitable for thermobarometrical calculations (Fig. 7b).

Application of an initial H_2O_{melt} input of 1.8 wt.% (primary input derived from plagioclase-melt hygrometry), P03 provides estimates of temperature between 1,106 and 1,140 °C (average = 1,118 °C; $n = 58$; $1\sigma = 9$ °C) and pressure between -425 and 237 MPa (average = 111 MPa; $n = 58$; $1\sigma = 65$ MPa). P08-32c generates pressure values between 139 and 554 MPa (average = 365 MPa; $n = 58$; $1\sigma = 91$ MPa) (Fig. 7e). Samples that yielded negative pressures were discounted during calculation of average P–T values. The application of secondary H_2O_{melt} inputs to model P03 does not alter these P–T estimates.

When clinopyroxene analyses from meta-basaltic (Group 1) xenoliths were tested, the 2007–2008 dome lava was found to be the most suitable equilibrium liquid, with



◀ **Fig. 6** Crystal size distribution (CSD) plots for mineral phases in the 2007–2008 lava dome. **a** Plagioclase CSDs show curved profiles, whilst **b** plagioclase microlite CSDs show straight slopes with a distinctive down-turn in the smallest crystal fraction. **c** Orthopyroxene CSDs show complex, kinked profiles. **d** Clinopyroxene CSDs exhibit curved profiles **e** Ti-magnetite CSDs show generally straight slopes. **f** Digitised thin sections for samples KLT-71a, Kelut-A and KLT-A, showing plagioclase, orthopyroxene, clinopyroxene, Ti-magnetite and vesicles **g** Digitised BSE image for sample Kelut-A, showing plagioclase microlites. **h** Digitised BSE image for sample KLT-71a, also showing plagioclase microlites

the majority of samples able to pass both of the previously applied equilibrium tests (Fig. 7c). Application of the previously described primary H_2O_{melt} input of 1.8 wt %, P03 provides P–T estimates between –720 and 237 MPa (average = 136 MPa; $n = 18$; $1\sigma = 243$ MPa), and 1,049 and 1,129 °C (average = 1,118 °C; $n = 18$; $1\sigma = 21$ °C), respectively. P08-32c produces a similar pressure range of –117 to 367 MPa (average = 231 MPa; $n = 19$; $1\sigma = 123$ MPa) (Fig. 7e).

Using clinopyroxene analyses from cumulate (Group 2) xenoliths, it was determined that Group 2 xenolith whole rock data are the most suitable representation of an equilibrium liquid (Fig. 7d). Using an initial H_2O_{melt} value of 8.3 wt.% (derived from amphibole hygrometry), P03 produces values in the range of 1,149–1,207 °C (average = 1,189 °C; $n = 21$; $1\sigma = 14$ °C) and 160–810 MPa (average = 620 MPa; $n = 21$; $1\sigma = 170$ MPa), whilst P08-32c calculates pressures between 640 and 1,150 MPa (average = 820 MPa; $n = 21$; $1\sigma = 140$ MPa).

Pressures and temperatures from clinopyroxene composition thermobarometry

The applied clinopyroxene thermometer (P08-32d) yields temperature estimates for the 2007–2008 dome lava between 1,116 and 1,173 °C (average = 1,150 °C; $n = 58$;

$1\sigma = 12$ °C). Temperatures derived from this model were then used as inputs for the clinopyroxene barometer (P08-32b), alongside an H_2O_{melt} value of 1.8 wt.% derived from plagioclase-melt hygrometry. This barometer calculates a total pressure range of 18–557 MPa (average = 317 MPa; $n = 58$; $1\sigma = 109$ MPa). Application of P08-32d/b to clinopyroxene found within meta-basaltic (Group 1) xenoliths, using the same H_2O_{melt} input, produces P–T estimates between –119 and 515 MPa (average = 246 MPa; $n = 19$; $1\sigma = 177$ MPa) and 798 and 1,166 °C (average = 1,103 °C; $n = 19$; $1\sigma = 94$ °C), respectively. Although temperature estimates remain unchanged by the application of secondary H_2O_{melt} values, a value of 0.9 wt.% yields an average pressure of 205 MPa, and a value of 2.6 wt.% produces an average pressure of 282 MPa.

Equilibrium tests for the cumulate (Group 2) xenoliths revealed that both dome lava whole rock and cumulate (Group 2) xenolith whole rock were suitable choices for melt compositions. When P08-32d/b is applied to cumulate (Group 2) xenolith clinopyroxenes, using 2007–2008 dome lava whole rock compositions, P–T estimates range from 1,060 to 1,199 °C (average = 1,136 °C; $n = 45$; $1\sigma = 25$ °C) and –49 to 427 MPa (average = 280 MPa; $n = 45$; $1\sigma = 113$ MPa). If the cumulate xenolith whole rock composition is used as a liquid composition, temperature results lie between 1,061 and 1,213 °C (average = 1,174 °C; $n = 21$; $1\sigma = 37$ °C), while the resulting pressures range from 253 to 842 MPa (average = 693 MPa; $n = 21$; $1\sigma = 157$ MPa).

P–T relationships and H_2O_{melt} from amphibole thermobarometry/hygrometry

Calculated pressures for amphibole-bearing xenoliths range from 569 to 650 MPa (average = 603 MPa; $n = 7$; SEE = ± 66 MPa; $1\sigma = 27$ MPa). Application of the

Table 5 CSD input parameters and results, including crystal habit and L_{max}

Sample	Mineral	Count	Crystal habit				Roundness	Shape	L_{max}	Phase proportion
			Short	Intermediate	Long	R^2 values				
KLT-71a	Plagioclase	1,221	1.00	1.50	2.60	0.88	0.3	Rectangular prism	1.55	30.6
KLT-71a	Orthopyroxene	234	1.00	1.50	3.00	0.52	0.3	Acicular	1.67	3.1
KLT-71a	Clinopyroxene	199	1.00	1.00	2.00	0.60	0.3	Rectangular prism	1.37	4.2
KLT-71a	Ti-magnetite	663	1.00	1.20	1.40	0.92	0.3	Rectangular prism	0.45	5.0
KLT-A	Plagioclase	396	1.00	1.25	2.00	0.65	0.3	Acicular	1.55	33.9
Kelut-A	Plagioclase	633	1.00	1.15	1.80	0.85	0.3	Rectangular prism	1.01	25.6
Kelut-A	Orthopyroxene	234	1.00	1.10	1.30	0.82	0.3	Acicular	0.82	7.5
Kelut-A	Clinopyroxene	201	1.00	1.60	2.10	0.84	0.3	Rectangular prism	1.67	6.4
Kelut-A	Ti-magnetite	204	1.00	1.15	1.30	0.86	0.3	Rectangular prism	0.45	3.0

Crystal habit is calculated using the *CSDSlice* methodology of Morgan and Jerram (2006). L_{max} is calculated by averaging the four largest crystals within each identified population

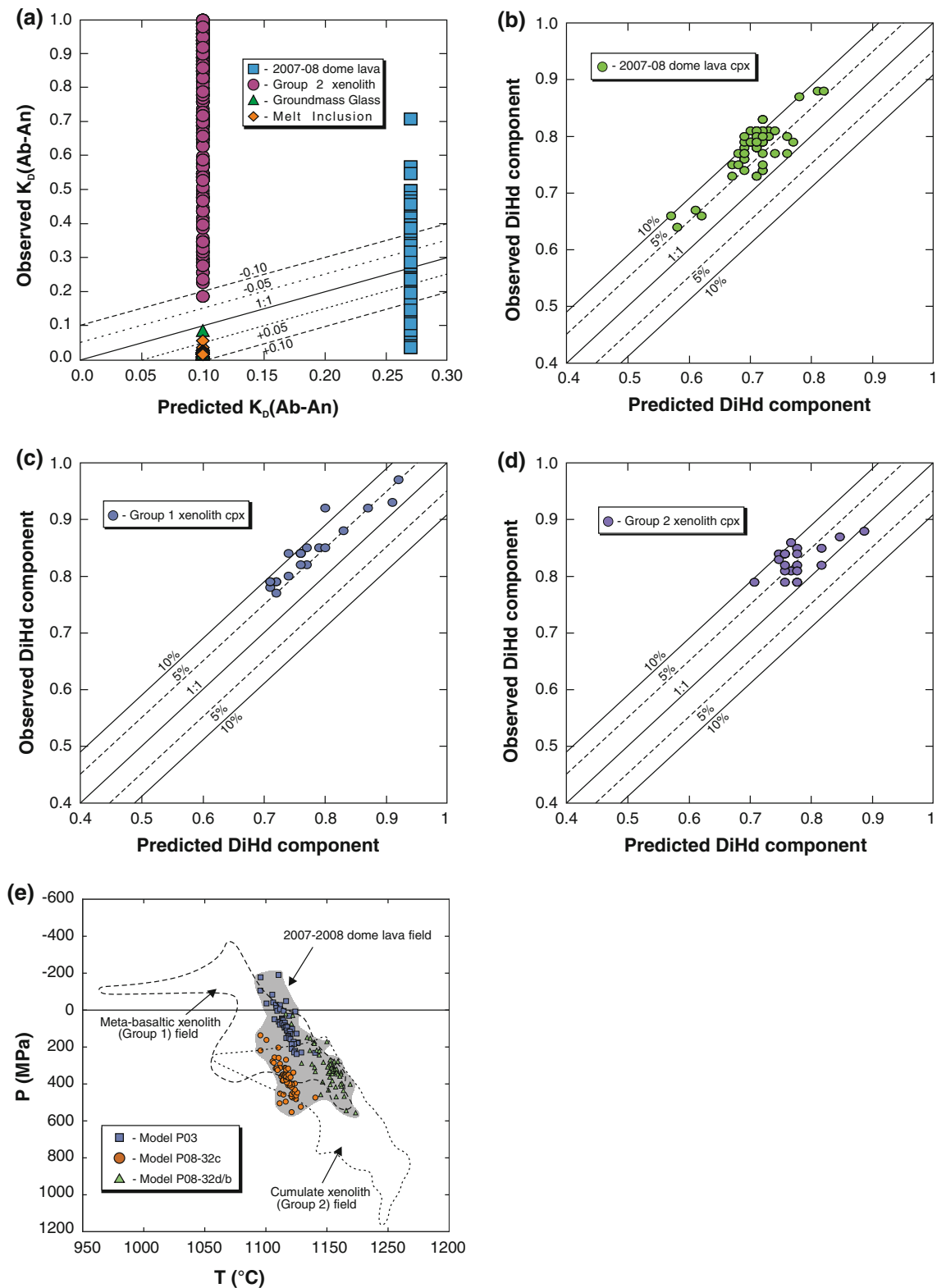


Fig. 7 **a** Equilibrium tests for the 2007–2008 dome lava plagioclase using the $K_D[\text{Ab-An}]$ (Putirka 2008). **b** Mineral DiHd equilibrium tests for 2007–2008 dome lava clinopyroxene and 2007–2008 dome lava whole rock. **c** Mineral DiHd component equilibrium tests between meta-basaltic xenolith (Group 1) clinopyroxene and the 2007–2008 dome lava whole rock. **d** Mineral DiHd component tests for

equilibrium between cumulate xenolith clinopyroxene (Group 2) and cumulate xenolith whole rock. **e** Pressure–temperature fields for 2007–2008 dome lava, alongside meta-basaltic and cumulate xenolith, derived from clinopyroxene barometry. *cpx* clinopyroxene, *Di* diopside, *Hd* hedenbergite, *Ab* albite, *An* anorthite

hygrometer provides H_2O_{melt} estimates between 8.1 and 8.6 wt.% (average = 8.3 wt.%; $n = 7$; $SEE = \pm 1.3$ wt.%; $1\sigma = 0.2$ wt.%). These are significantly higher than values acquired from plagioclase-melt hygrometers and suggest crystallisation from a significantly more hydrous melt than the 2007–2008 dome lava plagioclase. Calculated temperatures appear low when compared to temperature data previously acquired from plagioclase-melt, clinopyroxene-melt and clinopyroxene models, ranging from 992 to 1,005 °C (± 22 °C; average = 999 °C; $n = 7$; $SEE = \pm 22$ °C; $1\sigma = 4.5$ wt.%). Calculated oxygen fugacities range from $\Delta NNO = 0.7$ to 0.9 (average = 0.8; $n = 7$; $SEE = 0.4$; $1\sigma = 0.06$).

Discussion

Intensive variables and their implications for the magma plumbing system of the 2007–2008 Kelut eruption

The pressure estimates acquired above provide indications of the main magma storage zones and magma plumbing system within the crust below Kelut. Calculated pressures were converted to depths using a crustal density approximated from the inferred crustal stratigraphy (2,640 kg/m³) (Smyth et al. 2005, 2007). The three models applied to the 2007–2008 dome clinopyroxene define a broad region of crystallisation between 0 and 17 km, but with a bimodal distribution of pressure values. The first occurs at a depth of ~10 km, and the second at a depth of ~4 km. The latter appears less clearly defined, with a spread of clinopyroxene crystallisation throughout the upper crust (~2 to 7 km). This is a likely indicator of a complex system involving multiple magma storage zones throughout the upper crust and compares favourably with recent studies of the magma plumbing systems of other Indonesian arc volcanoes (e.g. Dahren et al. 2012; Chadwick et al. 2013; Preece et al. 2013a; Troll et al. 2013). The overlap in calculated temperature values provides a total range of 1,111–1,152 °C for this mid- to upper crustal system. This range correlates with temperature estimates produced via plagioclase thermometry (1,151–1,164 °C), implying that the majority of plagioclase crystallisation also occurs within the mid–upper crustal system. Plagioclase hygrometry provides an H_2O_{melt} estimate for this mid- to upper crustal system of 1.5 to 3.3 wt.% (average = 2.25 wt.%).

Meta-basaltic xenoliths (Group 1) produce an overall average depth value of 3.9 km, with a total range of 0 to 13.3 km. The high proportion of negative pressures produced is a likely representation of disequilibrium between the chosen melt composition (2007–2008 dome lava

whole rock) and the minerals used for thermobarometry, resulting from the significant variation in mineral assemblages, textures and compositions observed. Generally shallow depths, alongside an overall lower average temperature value of 1,102 °C, appear to constrain the meta-basaltic xenoliths to the upper crustal system, thus suggesting that these belong to chilled margin facies from shallow dyke and sill intrusions. Results acquired from cumulate xenolith (Group 2) clinopyroxene contrast strongly with those of meta-basaltic xenoliths, and produce an overall average depth of 18.4 km and a temperature of 1,182 °C. Amphibole barometry produces a similar average depth estimate of ~15.6 km, with a range of 14.7–16.8 km. These results overlap with the shallowest results derived from clinopyroxene barometry of Group 2 xenoliths and point to a storage region located in the deep crust (inferred Moho depth = 25 km; Guntoro 1999), potentially comparable to the ‘melting, assimilation, storage and homogenisation’ (MASH) zone of Hildreth and Moorbath (1988) or the ‘deep-crustal hot zone’ of Annen et al. (2006).

Magma dynamics beneath Kelut: petrographic indicators

Plagioclase textures

In the Kelut 2007–2008 dome, plagioclase sieve textures and oscillatory zonation are a common feature (Fig. 2a–d). Numerous theories as to the origin of sieve textures in plagioclase have been proposed, including mixing with a hotter or more mafic magma (e.g. Dungan and Rhodes 1978; Tsuchiyama 1985; Troll et al. 2004), rapid decompression (Nelson and Montana 1992) and skeletal growth during gas exsolution (Kuo and Kirkpatrick 1982). In the Kelut 2007–2008 dome lava, the melt inclusions that form sieve textures are predominantly elongate parallel to crystal faces and cross-cut polysynthetic twin planes, which allows skeletal growth to be ruled out. Nelson and Montana (1992) showed that coarse sieve textures could be generated by variations in pressure at constant temperature. Although similarly coarse sieve textures can be observed in the Kelut 2007–2008 dome (Fig. 2b), they are very rare compared to the fine-grained variety and restricted to the cores of the largest plagioclase phenocrysts. This observation suggests that decompression-driven resorption does indeed play a role in the system, but it is relatively minor in comparison with thermally driven resorption and occurred during the early stages of crystal growth.

The experiments of Tsuchiyama (1985) and Sunagawa (1992) illustrate that simple dissolution could be induced by an increase in melt temperature as little as 5–10 °C. When albite-rich crystals are immersed within a hotter melt

that is in equilibrium with a more anorthite-rich plagioclase, the ensuing reaction causes melt penetration of the crystal faces and formation of a fine-grained sieve texture (partial dissolution). Type 1 plagioclase crystals are therefore considered to have come into contact with a hotter, more mafic melt and thus provide likely evidence for mafic magma recharge and subsequent mixing processes. The presence of multiple sieve-textured zones within the largest crystals implies multiple mixing events prior to eruption. Where Type 1 plagioclase crystals exhibit a sieve-textured core, they are interpreted as examples of a greater degree of resorption, most likely through lengthy contact with a hotter, more mafic melt.

The presence of oscillatory zonation, with generally only small-scale compositional variations, suggests a regime of near-constant intensive parameters rather than the major change that might be expected from a magma-mixing event, or rapid depressurisation (e.g. Shore and Fowler 1996; Stewart and Fowler 2001; Landi et al. 2004; Shcherbakov et al. 2010). The relative abundance of oscillatory zonation compared to sieve-textured zones in the Kelut dome plagioclase population further strengthens the argument that in the Kelut magma plumbing system, oscillatory zonation results from long-term processes that are prevalent within the system rather than low-frequency, high impact events (e.g. Troll et al. 2004). The abundance of fairly small changes in An content between zones (<10 mol.%) implies relatively minor local disequilibrium rather than contact with a melt of significantly different composition (e.g. Troll and Schmincke 2002). The composition of plagioclase is strongly dependent upon melt temperature, water fugacity and melt composition. Although changes in pressure that exceed several kilobars are capable of altering plagioclase compositions (Nelson and Montana 1992), parameters such as H₂O fugacity are more severely affected by pressure changes, allowing even minor changes in pressure to indirectly alter plagioclase composition in volatile-rich magmas (Shcherbakov et al. 2010). Hygrometrical estimates of pre-eruptive H₂O_{melt} for the lower crustal system and the mid-to upper crustal system (8.1–8.6 wt.% and 1.5–3.3 wt.%, respectively) suggest that the magmas that fed the 2007–2008 eruption were hydrous, and therefore allowed the compositions of crystallising plagioclase to be altered during transportation within the relatively small vertical pressure gradient that might be expected within a single magma reservoir. As such, we interpret these zones as the result of crystal–liquid kinetics, arising from crystal movement within a thermally and compositionally zoned magma body, facilitated by convection currents (e.g. Homma 1932; Vance 1962; Hattori and Sato 1996; Ginibre et al. 2002a; Shcherbakov et al. 2010). Where boundaries between individual growth zones undulate, they are

considered an indicator of simple dissolution, and therefore the delicate balance between growth and subsequent resorption during convectational circulation (Pearce and Kolisnik 1990; Humphreys et al. 2006).

The zonation of iron in plagioclase provides a further indicator of pre-eruptive magmatic processes beneath Kelut. Iron is not a major element within plagioclase, but can be used as an indicator of processes such as melt differentiation, convection and magma recharge (Singer et al. 1995; Ginibre et al. 2002b; Troll and Schmincke 2002; Lundgaard and Tegner 2004). The Fe content of plagioclase is influenced by melt composition (Ginibre et al. 2002b; Ruprecht and Wörner 2007), oxygen fugacity, melt temperature, melt H₂O content and plagioclase An content (Bindeman et al. 1998; Wilke and Behrens 1999). Although other studies have shown either a positive correlation or no correlation between An and Fe content (Ruprecht and Wörner 2007; Shcherbakov et al. 2010; Mollo et al. 2011), the Kelut 2007–2008 dome plagioclase crystals show a negative correlation, with Mg and Fe contents of up to ~0.5 and ~2 wt.%, respectively, especially in zones of An depletion (down to ~An₄₅) (Supplementary material 3). This feature has also been observed in plagioclase phenocrysts from basaltic andesites of nearby Merapi volcano (Chadwick et al. 2007). Mollo et al. (2011) demonstrated that incorporation of Mg and Fe within plagioclase correlates positively with An content and is strongly controlled by cooling rate. However, the apparent decoupling of An with Mg and Fe observed within the 2007–2008 dome lava plagioclases suggests that an additional factor must play a role. Lundgaard and Tegner (2004) showed that the primary control upon partition coefficients for both Fe²⁺ and Fe³⁺ is melt composition, rather than oxygen fugacity or plagioclase composition. Oxygen fugacity ultimately affects Fe partitioning by controlling the proportions of Fe²⁺ to Fe³⁺ in the melt. However, when Fe²⁺/Fe³⁺ ratios were calculated stoichiometrically, no systematic variations were observed, either within individual crystals or across the entire 2007–2008 dome lava plagioclase population. This suggests that Fe-rich zones do not represent any significant change in oxygen fugacity. Such zones may therefore represent contact with a less evolved, more Fe- and Mg-rich melt during magma recharge and mixing events (e.g. Troll and Schmincke 2002). However, this fails to account for the low An content of these zones. An alternative explanation for the origin of low An, high Fe/Mg zones is the interaction of plagioclase phenocrysts with non-magmatic, crustal-derived melts, which are themselves the result of interaction between ascending magmas and upper crustal volcanoclastic sediment, calc-silicate material or crustal limestones (cf. Chadwick et al. 2007).

Mantled pyroxenes

Heterogeneous nucleation of clinopyroxene onto orthopyroxene may be an indicator of temperature increase resulting from the influx of a hotter magma or convective self-mixing (e.g. Nakagawa et al. 2002; Humphreys et al. 2009; Handley et al. 2010). The resorbed nature of many orthopyroxene cores may suggest that they were introduced to the shallow system during magma ascent from a deeper storage region and/or magma mixing. In this instance, resorption is envisaged to be the result of decompression during ascent, followed by nucleation and crystallisation of clinopyroxene. Alternatively, orthopyroxene phenocrysts may have originated within the shallow storage region, being resorbed by the influx of a hotter, more mafic magma. The textural complexity observed in both the general orthopyroxene population and the mantled pyroxene population suggests that both processes may play a role in the formation of mantled pyroxenes.

Meta-basaltic xenoliths and glomerocrysts

Textural observations such as rounded crystal morphologies in Group 1 xenoliths indicate partial re-melting. Where examples of lobate plagioclase and Ti-magnetite are found within clinopyroxene oikocrysts, they are interpreted as examples of preserved melt pockets. Clinopyroxene thermobarometry indicates that these xenoliths originated primarily within the upper crustal system (<10 km), and we therefore suggest that they represent upper crustal, chilled margin facies recycled from the margins of shallow dyke and sill intrusions.

Variations in dominant mineralogy and texture among the glomerocrysts observed within the dome lava suggest multiple sources. Complex patterns of oscillatory zoning and sieve textures are unlikely to be formed or preserved within cumulate phases for very long. As such, examples that include complexly zoned plagioclase crystals within the interior of the assemblage are interpreted as crystal clusters, composed of crystals that met and adhered to one another during convective circulation. Where glomerocrysts show textural similarity with meta-basaltic (Group 1) xenoliths (such as highly rounded crystals, outer layers of large, zoned plagioclase and hornfels textures), they are interpreted to result from partial disaggregation of meta-basaltic xenoliths (Group 1). Examples that exhibit no zonation are therefore considered to represent material that originally crystallised in situ within a thermal boundary zone. Outer crystals that exhibit zoning are considered to be magmatic in origin, having adhered to the glomerocrysts during convective circulation. In a few cases, an additional population of glomerocrysts is observed, typified by orthocumulate textures, containing polymineralic

assemblages that imply in situ crystallisation and a lack of exchange between interstitial liquid and magma chamber liquid. In these, clinopyroxene is commonly the cumulus phase, with plagioclase and minor Ti-magnetite as inter-cumulus phases. Such examples are considered to represent the recycled products of chilled margin thermal boundary zones.

Crustal xenoliths

Based on the studies of van Bemmelen (1949), Hamilton (1979), Guntoro (1999) and Smyth et al. (2005, 2007), the upper crust beneath Kelut comprises 8–11 km of recycled volcanoclastic crustal sediments derived from the arc itself, with minor shallow crustal limestones, underlain by a basement of metamorphosed arc and ophiolite material (e.g. metavolcanics and mafic intrusions). Meta-volcanoclastic xenoliths within the 2007–2008 lava dome provide evidence for incorporation and possible assimilation of upper crustal volcanoclastic sediment, whilst calc-silicate xenoliths imply interaction with upper crustal limestones. The shallow position of these limestones within the stratigraphic framework of Smyth et al. (2005) constrains the window of limestone assimilation and incorporation of older calc-silicate material to the uppermost crust.

Magma dynamics beneath Kelut: a quantitative textural perspective

Crystal size distribution trends

The majority of CSD plots for the 2007–2008 dome lavas display curved or kinked profiles, typically allowing for the presence of two separate slopes. Kinking or curvature of CSD slopes is often interpreted to result from processes such as textural coarsening, mixing of crystal cargoes and crystal accumulation (e.g. Higgins 1996; O'Driscoll et al. 2007). The degree of curvature provides a qualitative measure of the maturity of the mixing process, whereas the degree of kinking offers a qualitative measure of the overall complexity of the textural history (Cashman and Marsh 1988; Marsh 1998; Higgins 1996; Higgins 2006; Higgins and Roberge 2007). Previously described petrographical features suggest that the dominant mechanism for the generation of such CSD profiles is magma mixing. Higgins (2006) showed that magma mixing preserves the slopes of each component, regardless of their proportions. However, the value of the intercept and therefore the population density is lowered and no longer represents the true value. This observation suggests that although residence times can be derived from the slope values of the CSDs, calculations of parameters such as nucleation rate and population density will be inaccurate. The strong

petrographic evidence for resorption as a relevant process in the 2007–2008 dome lavas suggest that periods of crystallisation are missing from the textural record and as such, any residence times calculated from the CSD slopes are an absolute minimum.

The two distinct slopes for plagioclase (Fig. 6a) suggest two crystal populations. This division is verified by plotting slope intercept values against characteristic length, which produces distinctive clusters of larger and smaller plagioclase and Ti-magnetite size fractions (Supplementary material 6). The divisions of clinopyroxene and orthopyroxene in this way are fairly arbitrary and show that two slopes are probably not an entirely adequate representation of the complexity of pyroxene populations.

Residence times were calculated for each plagioclase slope using the method of Marsh (1988) and a selected growth rate of $1 \times 10^{-10} \text{ mm s}^{-1}$ (Higgins and Roberge 2007). Results range from 32 to 78 years for the larger population. These values imply that some plagioclase crystals may have experienced up to three of Kelut's previous eruptions while retained in the magma plumbing system. The smaller fractions produce residence times between 20 and 28 years, but the level of identified resorption suggests that they are not ideal for residence time calculations.

Straight slopes exhibited by plagioclase groundmass microlite CSDs are an indicator of a single nucleation event, likely a function of rapid crystallisation in response to ascent and eruption. Growth rates of plagioclase microlites are estimated to lie between 1×10^{-6} and $1 \times 10^{-8} \text{ mm s}^{-1}$ (Hammer et al. 1999; Brugger and Hammer 2010; Preece et al. 2013a). Using these growth rates, minimum and maximum crystallisation times were calculated and range from ~ 2 h to 9 days. Such crystallisation times suggest that microlite growth was late-stage, occurring during magma ascent and extrusion.

Complexly curved and kinked CSD profiles for orthopyroxene and clinopyroxene show that these phases also consist of multiple crystal populations that have in part undergone a complex textural history. Minimum residence times for the largest populations were calculated using a growth rate of $1 \times 10^{-8} \text{ mm s}^{-1}$ (cf. Burkhard 2005), yielding 100–270 days for orthopyroxene and 200–350 days for clinopyroxene. Such short growth times suggest that pyroxene (1) is extremely late-stage, (2) represents recycled constituents of cumulates derived from the magma chamber solidification fronts or (3) is subject to slower rates of growth than assumed in our calculation. Commonly observed orthocumulate textures suggest that some of these processes certainly occur, although we favour interpretations (2) and (3) to be the main reason for such low residence times. The heterogeneity of pyroxene textures, crystal sizes and CSDs provides evidence for recycling and re-incorporation of cumulate material, and

implies that no single growth rate is likely to be suitable for the entire pyroxene population of the 2007–2008 dome lava.

Ti-magnetite CSDs display simpler profiles, but, in the case of sample KLT-71a, can still be divided into two slopes. A lack of major compositional variation coupled with calculated residence times of 18–77 days would imply that Ti-magnetite crystals are the result of a single nucleation event. However, the curvature of the KLT-71a CSD provides evidence for multiple populations and suggests that a single growth rate may not be applicable. Considering that the dome could not be seen until approximately 30 days after the first evidence of imminent eruption, it seems plausible that one oxide population formed largely during final ascent, whilst another grew during shallow storage.

Integrating plagioclase petrography and crystal size distribution analysis

The CSD technique has been applied widely in igneous petrology to complement petrographical and geochemical observations and interpretations (Cashman 1988, 1991; Higgins 1996; Morgan et al. 2007; Higgins and Roberge 2007; O'Driscoll et al. 2007; Vinet and Higgins 2011). To test the validity of our petrographical interpretations, and relate qualitatively the different slopes of the plagioclase CSDs with the crystal textures observed in the 2007–2008 dome lava, sample KLT-71a was re-digitised to allow the distinction of plagioclase Types 1, 2 and 3. A single CSD plot for each of the three petrographic populations (Types 1, 2 and 3) was produced, whose slopes are labelled CSD₁, CSD₂ and CSD₃, respectively (Fig. 8c). These were then plotted alongside the total plagioclase CSD (CSD_{tot}) (Fig. 8a). A possible source of error that must be considered here is the overall crystal count. CSD₁ and CSD₂ are based upon 106 (15.08 % of total area) and 122 (6.07 % of total area) crystals, respectively, compared to 856 (4.28 % of total area) for CSD₃. Right-hand truncation effects might be expected to result from those with low crystal counts, caused by a disproportion of larger crystals compared to smaller ones. However, there is little evidence for this on the plots themselves, and few points were removed due to unacceptable errors.

Marsh (1988) showed that a curved CSD plot is the result of the interaction between two or more individual slopes. If the petrographic subdivisions are then related to the interpreted crystal populations identified from the CSDs, the CSD plots for each plagioclase type (CSD₁, CSD₂ and CSD₃) should link to slopes 1 and 2 of the plagioclase CSD (Fig. 8b). A diagram showing CSD₁, CSD₂ and CSD₃ plotted with CSD_{tot} is provided in Fig. 8a. Together, CSD₁, CSD₂ and CSD₃ produce a shape that is similar to CSD_{tot} and is defined by an upward-concave

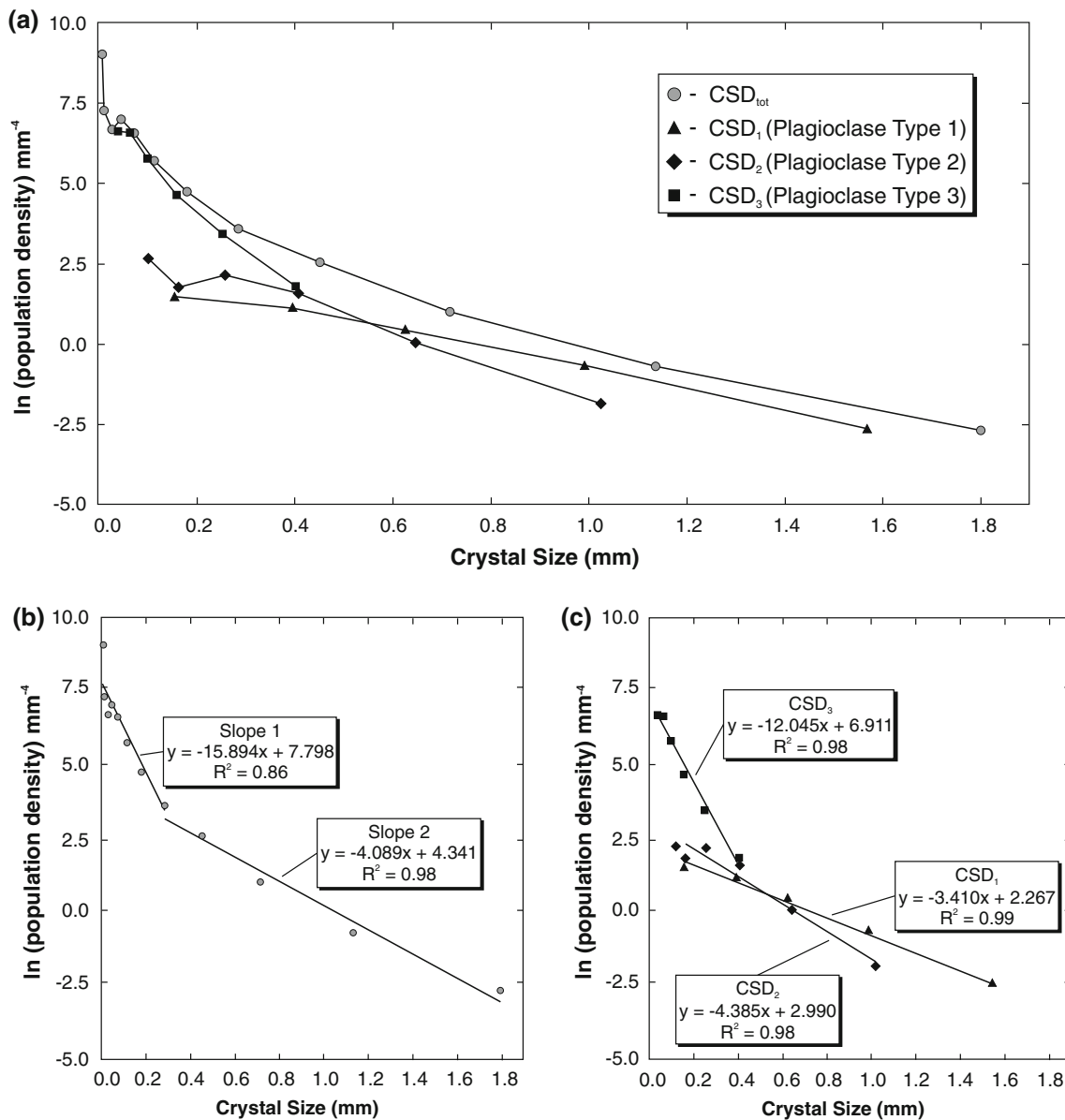


Fig. 8 **a** Total plagioclase CSD plotted against CSDs calculated for identified individual plagioclase populations. **b** Trendlines and slope values for interpreted size fraction populations of the total plagioclase

CSD. **c** Trendlines and slope values for CSDs calculated from interpreted petrographical plagioclase crystal populations

curve that dips below the profile of CSD_{tot} towards the middle. However, error bars associated with the largest fractions of CSD_3 and the smallest fractions of CSD_1 and CSD_2 are sufficiently large to account for this discrepancy.

The degree to which these individual CSDs fit the slopes of CSD_{tot} can be assessed quantitatively by comparing the slope equations derived from linear regressions of each CSD plot. A slope equation of $y = -4.089x \text{ mm} + 4.341 \text{ mm}^{-4}$ for Slope 2 (Fig. 8b) compares favourably with those of CSD_1 and CSD_2 ($y = -3.410x \text{ mm} + 2.267 \text{ mm}^{-4}$ and $y = -4.385x \text{ mm} + 2.990 \text{ mm}^{-4}$, respectively). This similarity suggests that Type 1 and 2 plagioclase phenocrysts are linked

with Slope 2 and are therefore two petrographically distinct members of the same crystal population. The slope equation for Slope 1 of Fig. 8b is given by $y = -15.894x \text{ mm} + 7.798 \text{ mm}^{-4}$, similar to the slope value of CSD_3 ($y = -12.045x \text{ mm} + 6.911 \text{ mm}^{-4}$).

The similarity between the crystal populations identified on the basis of textures and those identified by CSD shows that Slope 1 of the plagioclase CSDs (Fig. 8b) equates to Type 3 plagioclase micro-phenocrysts, whereas Slope 2 comprises both Type 1 and Type 2 phenocrysts, highlighting the petrological division between Types 3, and both Types 1 and 2. The representation of two texturally

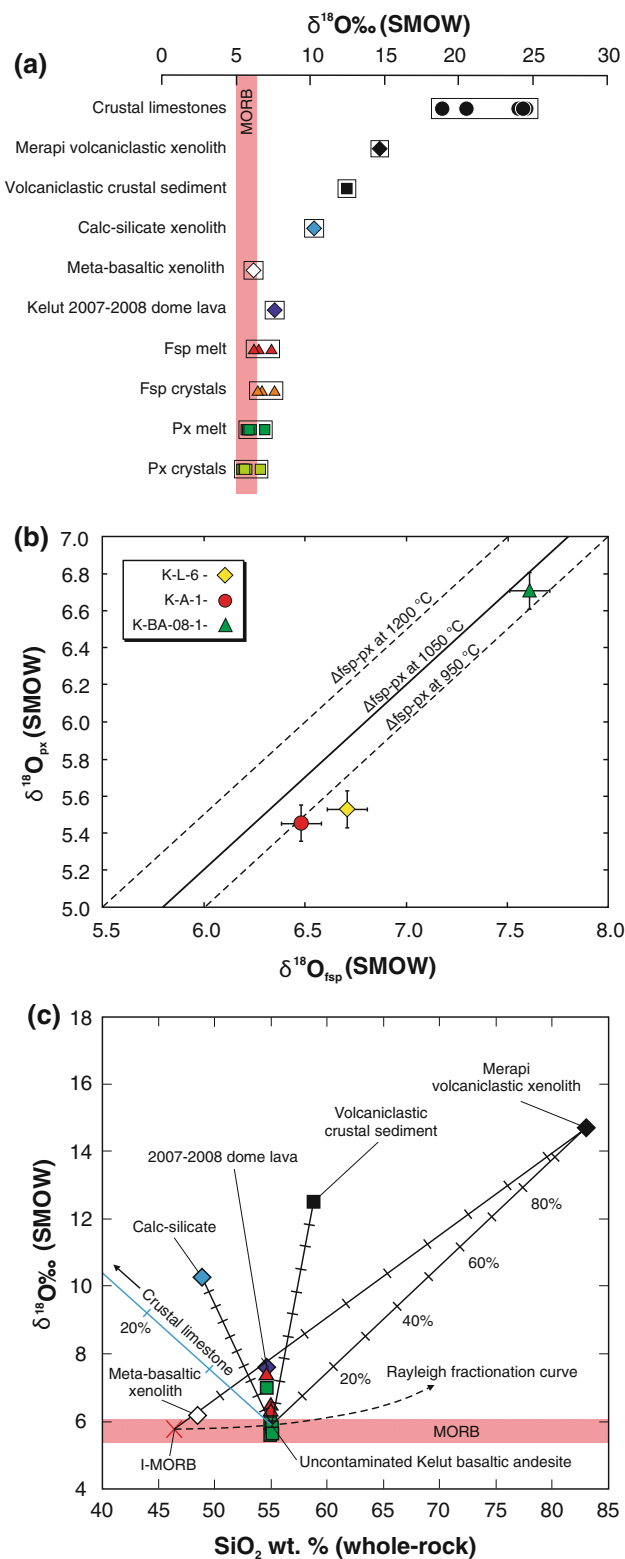


Fig. 9 Summary figure of whole rock $\delta^{18}\text{O}$ data for the 2007–2008 dome lava, crustal limestones (Gertisser and Keller 2003; Troll et al. 2012), a Merapi volcanoclastic xenolith (Troll et al. 2013), volcanoclastic crustal sediment (Troll et al. 2013), a Kelut calc-silicate xenolith and a meta-basaltic (Group 1) xenolith, also from Kelut. In addition, plagioclase and pyroxene $\delta^{18}\text{O}$ values are shown, with their corresponding magmatic $\delta^{18}\text{O}$ values. **b** Plot of $\delta^{18}\text{O}_{\text{fsp}}$ vs. $\delta^{18}\text{O}_{\text{px}}$ to test isotopic equilibrium. Isotherms calculated after Chiba et al. (1989). **c** Rayleigh fractionation model showing fractionation curve derived from the I-MORB values of Ito et al. (1987). Magma $\delta^{18}\text{O}$ values derived from pyroxenes and plagioclase are plotted alongside 2007–2008 dome lava whole rock and meta-basaltic and calc-silicate xenolith whole rock analyses. Binary mixing arrays are plotted between a basaltic andesite composition (55 wt.% SiO_2 , $\delta^{18}\text{O} = +5.9$) and potential contaminants (volcanoclastic sediment, average crustal limestone, calc-silicate xenolith). An additional mixing line between average I-MORB concentrations (Ito et al. 1987) and a Merapi volcanoclastic xenolith are also shown. Each tick mark represents 10 % of the crustal contaminant in the mixture

Magma dynamics beneath Kelut: isotopic constraints

Magma $\delta^{18}\text{O}$ values were calculated from plagioclase and pyroxene $\delta^{18}\text{O}$ values assuming values of $\Delta_{\text{fsp-melt}}$ and $\Delta_{\text{px-melt}}$ of +0.2 and -0.3 ‰, respectively, where $\Delta_{\text{mineral-melt}}$ is the per mil difference between mineral and magma at equilibrium (e.g. Kyser et al. 1981; Harris et al. 2005). Resulting $\delta^{18}\text{O}_{\text{fsp-melt}}$ values range from 6.2 to 7.4 ‰, which are moderately elevated relative to typical I-MORB values of 5.35 to 6.05 ‰ (average = 5.75 ± 0.3 ‰) (Ito et al. 1987) and MORB values of 5.7 ± 0.2 ‰ (Harmon and Hoefs 1995) (Table 4). Calculated $\delta^{18}\text{O}_{\text{px-melt}}$ values range from 5.7 to 7.0 ‰ and are either within the range of I-MORB values or slightly above (Fig. 9a).

The extent of O-isotopic equilibrium between co-existing minerals has been investigated by plotting average $\delta^{18}\text{O}$ values of plagioclase against those of pyroxene for each sample (Fig. 9b). Isotopic equilibrium between two minerals at the same temperature will result in a constant difference in $\delta^{18}\text{O}$ values between the two phases (e.g. Gregory and Criss 1986). As such, isotopic disequilibrium leads to data arrays that cut across calculated isotherms (Chiba et al. 1989). The Kelut data form a positive slope that appears to be broadly parallel to calculated isotherms, but deviates notably from the 1,150 °C isotherm, plotting close to the 950 °C isotherm instead. Estimates of crystallisation temperatures that typically cluster around 1,150 °C suggest that the 950 °C isotherm is not appropriate and that plagioclase and pyroxene are therefore not in isotopic equilibrium.

Closed-system Rayleigh fractionation modelling of the Kelut dome lava (Taylor and Sheppard 1986), assuming a primary, I-MORB-like, mantle-derived melt with an average SiO_2 value of 46.4 wt.% and $\delta^{18}\text{O}$ of 5.75 ‰ (Ito et al. 1987), shows that four of the five $\delta^{18}\text{O}_{\text{px-melt}}$ values lie within the range of typical I-MORB values (Ito et al. 1987),

distinct crystal populations (Types 1 and 2) by a single CSD slope (Slope 2) suggests that, in this case, the CSD is not as sensitive as the petrography and that the distinction of these two crystal populations lies effectively below the detection limit of the CSD.

and on the Rayleigh fractionation trend (Fig. 9c). One pyroxene gives a magma $\delta^{18}\text{O}$ value (7.0 ‰), that is somewhat higher than I-MORB values and cannot be produced from I-MORB via fractional crystallisation. This difference in magma $\delta^{18}\text{O}$ values can be explained by isotopic heterogeneity within the 2007–2008 dome lava pyroxene population, possibly derived from the mixing of pyroxenes from the lower or mid-crust, with pyroxenes that originated within the shallow crustal system. The pyroxenes with I-MORB-like $\delta^{18}\text{O}$ values are interpreted to have originated in the lower or mid-crust, where crustal contamination processes are negligible, assuming an isotopically distinct deeper crust. Alternatively, contamination may be masked by assimilation of lower or mid-crustal lithologies with similar $\delta^{18}\text{O}$ values to the magmas themselves. The pyroxene with a higher $\delta^{18}\text{O}$ value provides evidence for pyroxene crystallisation in the upper crust, where the presence of volcanoclastic sediments and limestones creates an isotopic contrast and therefore allows the detection of crustal contamination (see section “Geodynamic setting, geology and eruptive history of Kelut volcano”).

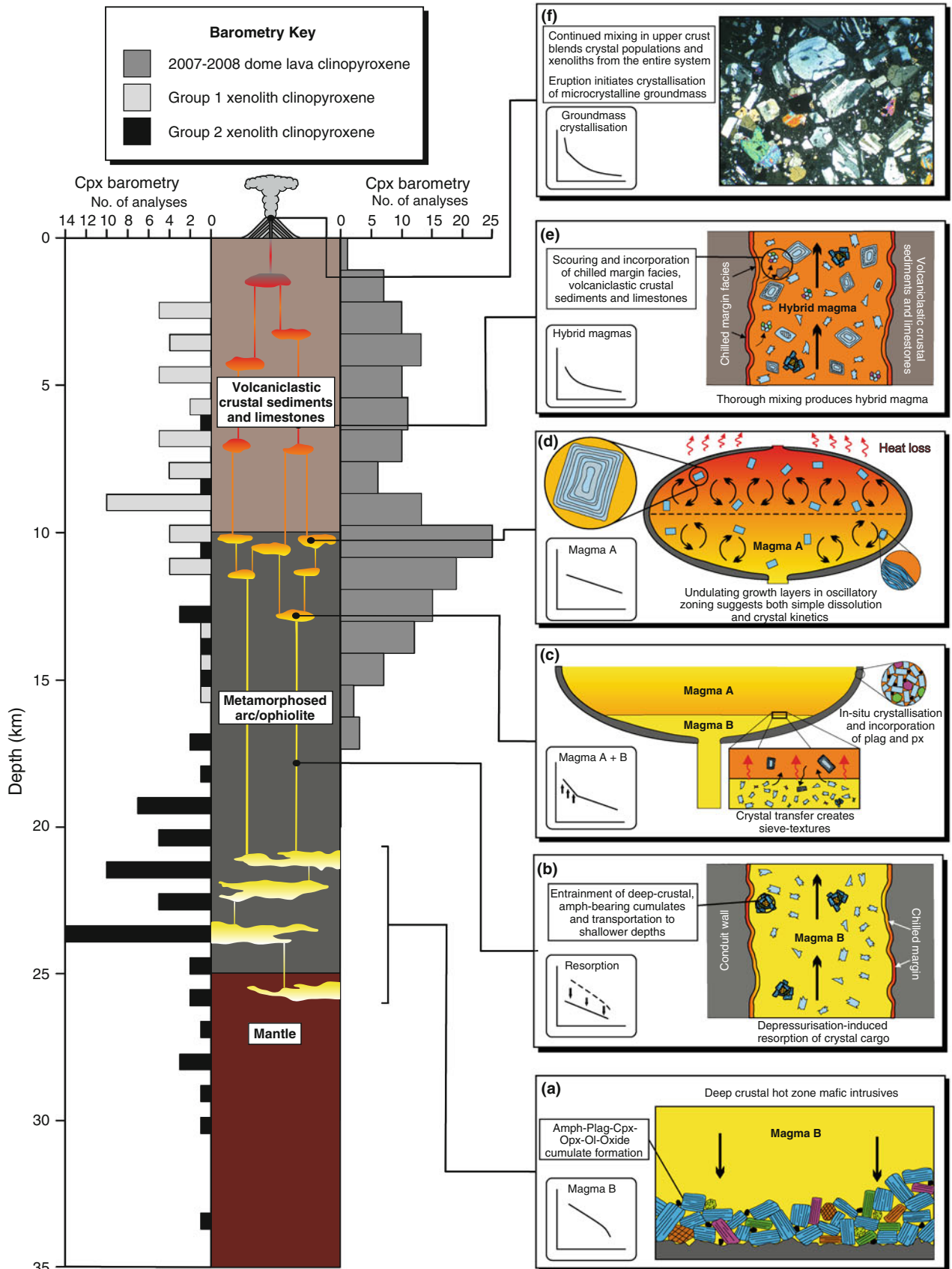
Magmatic $\delta^{18}\text{O}$ values calculated from plagioclase data vary between 6.2 and 7.4 ‰, and are all higher than the expected value for I-MORB or magmas derived from I-MORB via fractional crystallisation. The most likely explanation is that they have been affected by crustal contamination in the isotopically distinct upper crust. The single plagioclase with a higher magma $\delta^{18}\text{O}$ value (7.4 ‰) must therefore have been most affected by crustal contamination. The gap in magma $\delta^{18}\text{O}$ values calculated from plagioclase may highlight isotopic heterogeneity within the 2007–2008 dome lava plagioclase population, with higher $\delta^{18}\text{O}$ plagioclase crystals originating at shallower depths within the upper crust, where limestones and/or calc-silicate material may become a more significant contaminant (see section “Geodynamic setting, geology and eruptive history of Kelut volcano”). The contrast between magma $\delta^{18}\text{O}$ values recorded by plagioclase and pyroxene suggests that the former records a greater degree of crustal assimilation, although some effect of the selected fractionation factors or the small number of analyses cannot be excluded.

An analysed calc-silicate xenolith (Group 3) has a $\delta^{18}\text{O}$ value of 10.3 ‰, and although the calc-silicates are characterised by O-isotopic compositions that lie between mantle and typical Javanese upper crustal lithologies (cf. Gertisser and Keller 2003; Troll et al. 2013), they are considered here as a potential contaminant. This assumes that old calc-silicate (skarn) material could be assimilated after initial reaction with melt (e.g. Gaeta et al. 2009). Additional $\delta^{18}\text{O}$ values of a volcanoclastic xenolith from Merapi volcano (M-XCS-4; Troll et al. 2013),

volcanoclastic crustal sediment (J-VC-1; Troll et al. 2013) and limestone (carbonate) crust (Gertisser and Keller 2003; Troll et al. 2012) have been used as further potential contaminants, and as end-members for binary mixing models.

It is apparent from Fig. 9c that the Kelut samples do not fall on any mixing arrays between the proposed contaminants and a typical I-MORB composition. By contrast, the Kelut data plot within a mixing space between an uncontaminated Kelut basaltic andesite composition (55 wt.% SiO_2 ; $\delta^{18}\text{O} = 5.9$ ‰), volcanoclastic crustal sediment and calc-silicate, indicating that differentiation from basalt to basaltic andesite occurred prior to the onset of crustal contamination.

Binary bulk mixing of uncontaminated Kelut basaltic andesite with calc-silicate material shows that up to ~35 % contamination is required to explain the $\delta^{18}\text{O}$ values observed in the 2007–2008 dome lava. However, as pointed out above, the $\delta^{18}\text{O}$ values of calc-silicate xenoliths are likely to have been lowered during their interaction with silicate melt and consequent decarbonation (Valley 1986). As such, values on the order of ~35 % are considered to represent absolute maximum values for the degree of contamination. Significantly lower degrees of contamination of original limestone (with a $\delta^{18}\text{O}$ value of ~20 to 25 ‰) would be required to produce similar values to those observed in the Kelut 2007–2008 dome lava (<10 ‰), although the concomitant substantial decrease in whole rock SiO_2 concentrations is not observed. Using volcanoclastic crustal sediment as a contaminant, values of up to ~25 % contamination are required to produce the observed maximum magmatic $\delta^{18}\text{O}$ values of Kelut. These estimates of crustal contamination are significantly higher than those for nearby Merapi volcano, as suggested by Gertisser and Keller (2003) based on $\delta^{18}\text{O}$ – $^{87}\text{Sr}/^{86}\text{Sr}$ relationships (up to ~12 ‰), but are comparable to the estimates of Troll et al. (2013), based on $\delta^{18}\text{O}$ isotopic data alone. The former used local crustal limestones as potential contaminants, whilst the latter also presented mixing arrays with calc-silicates and crustal lithologies. At Kelut, none of the selected contaminants can account individually for the $\delta^{18}\text{O}$ values of the 2007–2008 dome lava. Instead, volcanoclastic crustal sediment, calc-silicates as well as crustal limestones may all play a role in the contamination of magmas at Kelut during storage in the upper crust. Given the relative abundance of volcanoclastic sediments over crustal limestones in the upper crustal stratigraphy beneath Kelut (van Bemmelen 1949; Hamilton 1979; Guntoro 1999; Smyth et al. 2005, 2007), we propose that volcanoclastic crustal sediment is the most significant contaminant of the 2007–2008 dome lava, with additional input from calc-silicate material and/or crustal limestones. This provides a contrast not only with Central Java, where shallow



◀ **Fig. 10** A conceptual model for magmatic processes and plumbing architecture beneath Kelut volcano. Schematic crustal stratigraphy derived from van Bemmelen (1949), Hamilton (1979), Guntoro (1999) and Smyth et al. (2007). Sequential development of observed CSD profiles is given where relevant. *Plag* plagioclase, *Px* pyroxene, *Opx* orthopyroxene, *Cpx* clinopyroxene, *Ol* olivine, *Amph* amphibole. **a** Stalling of melts derived from partial melting of the underlying mantle wedge, and formation of plagioclase–amphibole–clinopyroxene–orthopyroxene–olivine cumulates within a broad area between 20 and 25 km. **b** The ascent of magma to shallower levels recycles deep-crustal, amphibole-bearing cumulate nodules and causes intensive, decompressive resorption of the crystal cargo. **c** Mixing of ascending magmas with magmas that stalled in the transitional region between basement and overlying sediments, and continued to evolve in the mid-crust. Mixing with hotter, more primitive recharge magmas generates disequilibrium textures such as sieve textures and mantled pyroxenes. **d** Magmas in the mid-crustal storage zone continue to evolve and generate oscillatory zoning in the plagioclase cargo via, for example, convective self-mixing, disturbed periodically by ascending recharge magmas. **e** Ascent of mid-crustal magmas into a region of multiple magma storage zones within the upper crust promotes further mixing of crystal populations. Conduit margin material, comprising chilled margin facies and country rock (volcaniclastic crustal sediments, calc-silicate material, crustal limestones), is entrained within magmas and recycled/assimilated. **f** Eruption of a thoroughly mixed magma with a blended crystal cargo and xenoliths that represent much of the entire magma plumbing system. Eventually, most meta-basaltic xenoliths (Group 1) partially break down to produce glomerocrysts of varied mineral assemblages

crustal contamination is considered to be dominated by limestone (e.g. Chadwick et al. 2007; Deegan et al. 2010; Troll et al. 2013), but also with the Ijen Volcanic Complex (East Java), where processes of crustal contamination are considered to be negligible (Handley et al. 2007).

Magmatic processes beneath Kelut prior to the 2007–2008 eruption: an integrated model

A conceptual model for the present magma plumbing system beneath Kelut is given in Fig. 10. The variety of textures observed in the 2007–2008 dome lava requires the presence of a complex open-system magma plumbing system. Clinopyroxene–melt thermobarometry hints at two prominent magma storage zones; the first in the mid-crust (~10 km depth) and the second in the upper crust (<10 km depth). The former represents the majority of barometrical results obtained in this study and coincides with the approximate position of the boundary between the metamorphic basement and the overlying volcanoclastic sedimentary sequence (8–11 km depth, Smyth et al. 2005). This observation likely indicates stalling of ascending magmas near or at this boundary due to a density contrast. Textural complexity in the Kelut rocks and a broad distribution of pressure values that reflect shallow upper crustal storage indicate a complex regime of relatively small, interconnected magma pockets throughout the upper crust (< 10 km), with a possible magma plexus at a depth of ~4 km.

Upward migration of primary magmas

We envisage the generation and upward migration of primary (mantle-derived) hydrous basaltic magmas beneath Kelut. These magmas stall around the crust–mantle boundary (~25 km depth) and solidify in part as basic intrusions through crystallisation of calcic plagioclase, clinopyroxene, orthopyroxene, olivine and amphibole forming cumulates (Fig. 10a). Estimates of 8.3 ± 1.3 wt.% H₂O for the melt in equilibrium with cumulate (Group 2) xenoliths are comparable to other estimates of H₂O contents of primary subduction zone magmas (e.g. Sisson and Layne 1993; Roggensack et al. 1997; Wallace 2005; Humphreys et al. 2008; Blundy et al. 2010; Kelley et al. 2010). However, this water content is shown to decrease to between 1.5 and 3.3 wt.% just prior to eruption. We suggest that these lower crustal, amphibole-bearing cumulates play some role in the removal of water from hydrous, mantle-derived melts that stall in the lower crust (e.g. Davidson et al. 2007), but will in turn liberate H₂O on reincorporation into the active magma system. Magmatic degassing during ascent to shallower crustal levels is also envisaged to alter the H₂O content of the melt and is possibly the greater control on pre-eruptive H₂O content.

Eventually, these mafic to intermediate magmas rise through the deep crust and stall in the mid-crust, at the boundary between the metamorphic basement and the overlying volcanoclastic sedimentary sequence. Plagioclase–clinopyroxene–orthopyroxene–amphibole–olivine cumulate xenoliths are recycled into the magma and transported upwards at this stage, and depressurisation forces solid phases (e.g. plagioclase) above their liquidus, thus promoting extensive resorption (Fig. 10b).

Magma mixing and formation of sieve textures

Phenocryst textures alongside CSD profiles indicate the operation of magma mixing as a significant process within the Kelut plumbing system. The proposed driving forces behind magma mixing can be variable, including convective self-mixing (e.g. Couch et al. 2001; Troll and Schmincke 2002), injection of new magma (e.g. Sparks et al. 1977; Huppert and Sparks 1980) and mixing within the conduit during eruption (e.g. Snyder and Tait 1995; Wiesmaier et al. 2011).

The Fe–Mg-rich zones observed in plagioclase traverses imply contact with a more mafic hydrous melt. It is therefore suggested that continued fractional crystallisation in mid-crustal storage zones increases the thermal and compositional contrast between deep-crustal and mid-crustal magmas, to create the basaltic andesite magma that extruded in 2007–2008. Ascending hotter, more mafic and more hydrous deep-crustal magmas are likely introduced

periodically to the mid-crustal level. Contact of plagioclase formed in the mid-crustal zone with these magmas promotes partial dissolution and generation of sieve textures that define Type 1 plagioclase (e.g. Dungan and Rhodes 1978; Tsuchiyama 1985) (Fig. 10c). Examples of ‘spongy cores’ are considered to represent crystals that were entirely incorporated into the intruding magma and underwent accelerated thermal resorption (Troll et al. 2004; Humphreys et al. 2006). Additionally, heavily resorbed mineral phases that originated in the deep-crustal zone are dispersed into more evolved mid-crustal magmas, leading to the resorbed crystal cores observed within Type 1 and 2 plagioclase crystals, and nucleation of clinopyroxene on pre-existing orthopyroxenes. Rhyolitic melt inclusions within sieve-textured zones in plagioclase may imply that the main magmatic evolution occurs in this mid-crustal storage zone.

If the injected magma (magma B) is less dense than the resident magma (magma A) (Fig. 10), turbulent fountaining will lead to rapid dispersal and disaggregation of magma B and generate magmatic enclaves exhibiting chilled margins (Campbell 1996; Coombs et al. 2002). However, no magmatic enclaves were found within the 2007–2008 dome and CSDs slopes are generally curved, suggesting fairly complete and steady-state mixing rather than mingling processes in operation at this level.

If magma B is denser than magma A, basal flow and underplating of magma A will occur, providing a heat source that drives thermal convection (Huppert and Sparks 1980; Snyder and Tait 1995; Couch et al. 2001; Troll et al. 2004). A diffusive interface may then form between the two magmas, with heat being transferred to, and driving convection in magma A, whilst slowly leading to large-scale mixing (Turner and Campbell 1986; Eichelberger et al. 2000) (Fig. 10c).

Plagioclase crystals without sieve textures (Type 2) are considered to have remained separated from rejuvenating melts, either by evolving in a magma pocket that did not experience magma mixing or, alternatively, by being located at the top of a storage chamber or pocket and hence not significantly affected by mixing. Crystals situated in the upper portions of the chamber are unlikely to sink through multiple diffusive layers and are therefore considered to continue to grow with oscillatory zoning that reflects small variations in P–T conditions only. The presence of multiple sieve-textured zones within individual crystals suggests that parts of this mid-crustal storage zone may be subject to regular mixing events. Type 1 and Type 2 plagioclase are therefore considered to be products of the mid-crustal magma storage zone, and hence, they record a range of different processes. This agrees with CSD analyses, which indicate a strong similarity between the two crystal types, while Type 3 plagioclase micro-phenocrysts are markedly different.

Convective self-mixing and oscillatory zoning

Previous authors have shown that convection within magma bodies represents an important controlling factor for magma dynamics at depth and can be driven by a wide variety of processes (e.g. Huppert and Sparks 1984; Brandeis and Jaupart 1986; Martin et al. 1987). Worster et al. (1990) showed that vigorous convection can be initiated without the need for superheating, instead being generated by processes such as heat loss through the chamber roof or crystallization. Figure 10d illustrates how conduction of heat through the chamber roof in the Kelut magma plumbing system creates a negative buoyancy in the upper chamber, thus driving temperature-controlled convective currents. Plagioclase crystals within the main magma body are entrained within magma convection currents, transporting them through minor temperature and pressure gradients and causing the growth of oscillatory zones in conjunction with simple dissolution. As such, oscillatory zonation represents periods of ‘background’ activity within a slowly cooling magma chamber or pocket and leads to the generation of Type 2 plagioclase crystals. The considerable variation in textures between Type 1 and 2 plagioclase crystals, coupled with the CSD evidence that they both originate within the mid- to upper crustal system, implies that the reservoir(s) must have been sufficiently heterogeneous to allow for a variety of pre-eruptive processes. We suggest that compositional and thermal gradients may be large enough to generate double-diffusive layering, developing chambers and pockets that are stratified (Fig. 10d).

During turbulent convective periods, driven by injection of magma from deep zones, cumulus material and chilled margin material are recycled into the melt body and subject to disaggregation, creating multiple populations of clinopyroxene and orthopyroxene and generating the complex CSD slopes observed in Fig. 6c, d.

Continued ascent, xenolith incorporation and degassing

It is envisaged that mid-crustal magmas eventually ascend into, and stall within, the upper crust. Clinopyroxene barometry indicates relatively evenly distributed crystallisation throughout the upper crust, implying multiple magma storage pockets, in which magmas of broadly similar composition slowly ascend, perhaps stalling in one broad region before final ascent. Similar concepts have been suggested for other Indonesian volcanoes such as Merapi (Troll et al. 2013; Preece et al. 2013a) and Krakatau (Dahren et al. 2012; Gardner et al. 2013). Upper crustal residence continues the trend of evolution towards rhyolite and promotes thorough mixing of multiple crystal populations. Meta-basaltic (Group 1) and calc-silicate (Group 3)

xenoliths are incorporated and/or assimilated within this upper crustal region (as defined by stratigraphy and clinopyroxene barometry) (Fig. 10e).

Calculated H₂O contents range from ~1.5 to 3.3 wt.%, while melt inclusion Cl and S concentrations show 2,000 to 4,000 and <200 ppm (Table 3), respectively. These data suggest that pre-eruptive volatile concentrations of the 2007–2008 dome lava are comparable to other dome-forming, subduction-type volcanoes such as Merapi, Shiveluch and Colima (e.g. Blundy et al. 2006; Humphreys et al. 2006; Savov et al. 2008, Preece et al. 2013b). Significantly lower volatile concentrations in groundmass glass (e.g. Cl = <2,500 ppm and average estimated H₂O = 0.4 wt.%; n = 14; 1σ = 0.3) indicate considerable loss of volatiles during final ascent and eruption. Assuming a depth to the shallow storage zone of ~4 km and utilising the time gap of 1 month between initial indications of increased activity from the monitoring record and first observations of the lava dome, a magma ascent rate of 0.0015 m/s can be inferred for the 2007–2008 eruption (Siebert et al. 2011). Anomalous CO₂ fluxes observed up to 4 months prior to the first stages of the eruption may represent the influx of a hot, volatile-rich magma into the shallow storage system, or the liberation of crustal volatiles from such rejuvenation. If this point in time is taken instead to mark magma ascent, the inferred ascent rate is calculated at 0.0004 m/s.

Explosive versus effusive eruptive behaviour at Kelut: hazard implications

Similarities between major and trace element compositions of the 1990 and 2007–2008 eruptions imply that the contrasting eruption styles of Kelut are not the result of geochemical variation. We suggest that differences in degassing behaviour, as a function of ascent rate, are likely to play a significant role in the eruptive behaviour of the volcano, as suggested for similar andesitic systems such as Mt. Pelee (e.g. Martel et al. 2000), Taranaki (e.g. Platz et al. 2007) and Merapi (e.g. Gertisser et al. 2011; Preece et al. 2013a).

More locally, the reduction in volume of the Kelut crater lake during lava dome extrusion in 2007–2008 has important implications for ongoing hazard management in the surrounding area. At present, the threat of primary, hot lahars has been temporarily removed, rendering Kelut volcano less hazardous compared to its volcanic history of deadly lahar-forming eruptions that have caused more than 15,000 deaths since A.D. 1500. The presence of relict lava domes at the summit of the Kelut edifice implies that lava dome extrusion may be cyclic, with periods of high explosivity and the presence of a substantial crater lake that transition into short periods of effusive activity and crater

lake displacement. Explosive phases are known historically to have not only generated devastating lahars, but also to have widened and deepened the crater lake, increasing the overall volume of water that can be available for lahar generation. As shown in 2007–2008, effusive activity can counteract this by gradually removing the crater lake and infilling the crater with dome material. In August 2012, the remaining crater lake was estimated to be only ~1 × 10³ m³ in volume (A. Bernard pers. comm. 2012), which contrasts with the pre-2007 lake volume of 2.1 × 10⁶ m³. The absence of a significant crater lake lessens the potential for Kelut to produce large-scale primary lahars and suggests that, at least until such time as the dome is removed and the crater lake fully re-established, Kelut's greatest hazard is mitigated. With an average rainfall of 5–7 × 10⁶ m³/year, Kelut's crater lake is theoretically capable of refilling within a few years of an eruption, as shown by measured rates of lake level rise of up to 5 cm per day following the 1990 eruption (Siebert et al. 2011). However, it appears that the presence of the new 2007–2008 dome in the crater has inhibited the development of a significant crater lake during the past 5-year period since the 2007–2008 eruption.

Conclusions

The Kelut 2007–2008 lava dome provides evidence for a complex magma system that comprises a deep-crustal storage region, a mid-crustal storage zone and a diffuse, upper crustal zone, likely made up of multiple magma storage zones and pockets. Crystal size distributions indicate that mixing processes occur in the mid- to upper crustal system, combining multiple texturally distinct plagioclase populations. Complex zonation, disequilibrium textures and Fe-rich crystal zones observed in the shallow crystal populations indicate both convection of stored magmas and interaction of older, shallower magmas with hotter magmas from depth. Recharge magmas may contain resorbed crystal cargoes and cumulate xenoliths, indicating crystal recycling and decompression-induced resorption, hence contributing to the overall textural diversity of the Kelut eruptive products. Multiple disequilibrium textures preserved within single plagioclase crystals indicate multiple magma mixing events and incremental evolution in the upper crustal storage region prior to eruption. Calculated magma H₂O contents range from ~8.1 to 8.6 wt.% in the deep storage region and decrease to ~1.5 to 3.3 wt.% in the mid- to upper crustal region. Estimated ascent rates of 0.0015 m/s and 0.0004 m/s facilitate degassing of the 2007–2008 magma batch already in the conduit, allowing protracted volatile escape via permeable conduit wall rocks, and thus likely limiting the eruption style to effusion.

Oxygen isotopic data are either similar or moderately elevated relative to typical I-MORB values and can be explained by assimilation of upper crustal material, including volcanoclastic crustal sediments, calc-silicates and limestones. Variations in $\delta^{18}\text{O}$ - SiO_2 space indicate that none of these potential contaminants can account independently for the $\delta^{18}\text{O}$ variations observed in the Kelut 2007–2008 eruption. Instead, a combination of both volcanoclastic sediment and calc-silicate (and/or limestone) contamination is required by our data, with a likely predominance of the former given the abundance of recycled, arc-derived volcanoclastic sediment in the upper crust of East Java. Variations in calculated magma $\delta^{18}\text{O}$ values from pyroxenes (5.7–7.0 ‰) and plagioclase (6.2–7.4 ‰), alongside isotopic disequilibrium between plagioclase and pyroxene suggest multiple populations of crystals that originate from different depths within the magma system. Binary bulk mixing models indicate that differentiation from basalt to basaltic andesite largely occurred prior to any assimilation of isotopically distinct, upper crustal material, whilst the evolved magma compositions observed in melt inclusions and groundmass glass suggest that differentiation towards rhyolitic compositions must have occurred within the mid- to upper crustal system.

Regarding the hazards that Kelut volcano poses to the surrounding population, the gradual growth of a lava dome during the 2007–2008 events has resulted in the displacement of the crater lake, which has temporarily removed Kelut's most acute hazard, namely the generation of primary, hot lahars.

Acknowledgments We are grateful to the Research Institute for the Environment, Physical Sciences and Applied Mathematics (EPSAM), Keele University, for use of facilities and financial support. We acknowledge our colleagues from the Merapi Volcano Observatory (BPPTK) in Yogyakarta for their support over many years. We thank L. Schwarzkopf, L. Blythe and F. Deegan for assistance during fieldwork, Sony for sample collection at Kelut and M. Mahjum for logistical support. F. Rawoot is thanked for her help with the O-isotope analyses. A. Kronz (University of Göttingen, Germany) kindly provided access to the electron microprobe facility at Göttingen and analytical support. We are grateful for the insightful, detailed and constructive reviews by E. Hildner and H. Handley. In-kind contributions from The Open University and financial support from the Swedish Research Council (VR), the Royal Swedish Academy of Sciences (KVA) and the Centre for Natural Disaster Sciences (CNDS) at Uppsala University are gratefully acknowledged.

References

- Annen C, Blundy JD, Sparks RSJ (2006) The genesis of intermediate and silicic magmas in deep crustal hot zones. *J Petrol* 47:505–539
- Barker AK, Troll VR, Ellam RM, Hansteen TH, Harris C, Stillman CJ, Andersson A (2012) Magmatic evolution of the Cadamosto Seamount, Cape Verde: beyond the spatial extent of EM1. *Contrib Mineral Petrol* 163:949–965
- Bindeman IN, Davis AM, Drake MJ (1998) Ion microprobe study of plagioclase-basalt partition experiments at natural concentration levels of trace elements. *Geochim Cosmochim Acta* 62:1175–1193
- Blundy J, Cashman K (2001) Ascent-driven crystallisation of dacite magmas at Mount St Helens, 1980–1986. *Contrib Mineral Petrol* 140:631–650
- Blundy J, Cashman K, Humphreys M (2006) Magma heating by decompression-driven crystallisation beneath andesite volcanoes. *Nature* 443:76–84
- Blundy J, Cashman KV, Rust A, Whitham F (2010) A case for CO_2 -rich arc magmas. *Earth Planet Sci Lett* 290:289–301
- Boorman S, Boudreau A, Kruger FJ (2004) The lower zone-critical zone transition of the Bushveld Complex: a quantitative textural study. *J Petrol* 45:1209–1235
- Bourdier J-L, Pratomo I, Thouret J-C, Boudon G, Vincent PM (1997) Observations, stratigraphy and eruptive processes of the 1990 eruption of Kelut volcano, Indonesia. *J Volcanol Geotherm Res* 79:181–203
- Brandeis G, Jaupart C (1986) On the interaction between convection and crystallization in cooling magma chambers. *Earth Planet Sci Lett*, pp 345–361
- Brugger CR, Hammer JE (2010) Crystallization kinetics in continuous decompression experiments: implications for interpreting natural magma ascent processes. *J Petrol* 51:1941–1965
- Burkhard DJM (2005) Nucleation and growth rates of pyroxene, plagioclase and Fe–Ti oxides in basalt under atmospheric conditions. *Eur J Mineral* 17:675–685
- Campbell IH (1996) Fluid dynamic processes in basaltic magma chambers. In: Cawthorn RG (ed) *Layered Intrusions*, Elsevier Science, p 531
- Cashman KV (1988) Crystallization of Mount St. Helens 1980–1986 dacite: a quantitative textural approach. *Bull Volcanol* 50:194–209
- Cashman KV (1991) Groundmass crystallization of Mount St. Helens dacite, 1980–1986: a tool for interpreting shallow magmatic processes. *Contrib Mineral Petrol* 109:431–449
- Cashman KV, Marsh BD (1988) Crystal size distribution (CSD) in rocks and the kinetics and dynamics of crystallization, II. Makaopuhi lava lake. *Contrib Mineral Petrol* 99:292–305
- Caudron C, Mazot A, Bernard A (2012) Carbon dioxide dynamics in Kelut volcanic lake. *J Geophys Res* 117:B05102
- Chadwick JP, Troll VR, Ginibre C, Morgan D, Gertisser R, Waight T, Davidson JP (2007) Carbonate assimilation at Merapi Volcano, Java, Indonesia: insights from crystal isotope stratigraphy. *J Petrol* 48:1793–1812
- Chadwick JP, Troll VR, Waight TE, van der Zwan FM, Schwarzkopf LM (2013) Petrology and geochemistry of igneous inclusions in recent Merapi deposits: a window into the sub-volcanic plumbing system. *Contrib Mineral Petrol* 165:259–282
- Chiba H, Chacko T, Clayton RN, Goldsmith JR (1989) Oxygen isotope fractionations involving diopside, forsterite, magnetite, and calcite: application to geothermometry. *Geochim Cosmochim Acta* 53:2985–2995
- Coombs ML, Eichelberger JC, Rutherford MJ (2002) Experimental and textural constraints on mafic enclave formation in volcanic rocks. *J Volcanol Geotherm Res* 119:125–144
- Cooper KM, Reid MR (2003) Re-examination of crystal ages in recent Mt St Helens lavas: implications for magma reservoir processes. *Earth Planet Sci Lett* 213:149–167
- Couch S, Sparks RSJ, Carroll MR (2001) Mineral disequilibrium in lavas explained by convective self-mixing in open magma chambers. *Nature* 411:1037–1039
- Dahren B, Troll VR, Andersson UB, Chadwick JP, Gardner MF, Jaxybulatov K, Koulakov I (2012) Magma plumbing beneath

- Anak Krakatau volcano, Indonesia: evidence for multiple magma storage regions. *Contrib Mineral Petrol* 163:631–651
- Davidson JP, Tepley FJ (1997) Recharge in volcanic systems: evidence from isotopic profiles of phenocrysts. *Science* 275:826–829
- Davidson J, Turner S, Handley H, Macpherson C, Dosseto A (2007) Amphibole “sponge” in arc crust? *Geology* 35:787–790
- De Bézal E, Lavigne F, Gaillard JC, Grancher D, Pratomo I, Komorowski JC (2012) The 2007 eruption of Kelut volcano (East Java, Indonesia): phenomenology, crisis management and social response. *Geomorphology* 136:165–175
- Deegan FM, Troll VR, Freda C, Misiti V, Chadwick JP, McLeod CL, Davidson JP (2010) Magma-carbonate interaction processes and associated CO₂ release at Merapi volcano, Indonesia: insights from experimental petrology. *J Petrol* 51:1027–1051
- Devine JD, Gardner JE, Brack HP, Layne GD, Rutherford MJ (1995) Comparison of microanalytical methods for estimating H₂O contents of silicic glasses. *Am Mineral* 80:319–328
- Drake MJ (1976) Plagioclase-melt equilibria. *Geochim Cosmochim Acta* 40:457–465
- Dungan MA, Rhodes JM (1978) Residual glasses and melt inclusions in basalts From DSDP Legs 45 and 46: evidence for magma mixing. *Contrib Mineral Petrol* 67:417–431
- Edwards CMH, Menzies MA, Thirlwall MF, Morris JD, Leeman WP, Harmon RS (1994) The transition to potassic alkaline volcanism in island arcs: the Ringgit-Beser Complex, East Java, Indonesia. *J Petrol* 35:1557–1595
- Eichelberger JC, Chertkoff DG, Dreher ST, Nye CJ (2000) Magmas in collision: rethinking chemical zonation in silicic magmas. *Geology* 28:603–606
- Elliott MT, Cheadle MJ, Jerram DA (1997) On the identification of textural equilibrium in rocks using dihedral angle measurements. *Geology* 25:355–358
- Fagereng A, Harris C, La Grange MS, Stevens G (2008) Stable isotope study of the Archaean rocks of the Vredefort impact structure, central Kaapvaal Craton, South Africa. *Contrib Mineral Petrol* 155:63–78
- Foden JD (1982) The petrology of the calcalkaline lavas of Rindjani volcano, East Sunda Arc: a model for island arc petrogenesis. *J Petrol* 24:98–130
- Gaeta M, Di Rocco T, Freda C (2009) Carbonate assimilation in open magmatic systems: the role of melt-bearing skarns and cumulate-forming processes. *J Petrol* 50:361–385
- Gamble JA, Price RC, Smith IEM, McIntosh WC, Dunbar NW (2003) ⁴⁰Ar/³⁹Ar geochronology of magmatic activity, magma flux and hazards at Ruapehu volcano, Taupo Volcanic Zone, New Zealand. *J Volcanol Geotherm Res* 120:271–287
- Gardner MF, Troll VR, Gamble JA, Gertisser R, Hart GL, Ellam RM, Harris C, Wolf JA (2013) Shallow level differentiation processes at Krakatau: evidence for late-stage crustal contamination. *J Petrol* 54:149–182
- Gerbe M-C, Gourgaud A, Sigmarsson O, Harmon RS, Joron J-L, Provost A (1992) Mineralogical and geochemical evolution of the 1982–1983 Galunggung eruption (Indonesia). *Bull Volcanol* 54:284–298
- Gertisser R, Keller J (2003) Trace element and Sr, Nd, Pb and O isotope variations in medium-K and high-K volcanic rocks from Merapi volcano, central Java, Indonesia: evidence for the involvement of subducted sediments in Sunda arc magma genesis. *J Petrol* 44:457–489
- Gertisser R, Charbonnier SJ, Troll VR, Keller J, Preece K, Chadwick JP, Barclay J, Herd RA (2011) Merapi (Java, Indonesia): anatomy of a killer volcano. *Geol Today* 27:57–62
- Ghiorso MS, Hirschmann MM, Reiners PW, Kress VC III (2002) The pMELTS: a revision of MELTS for improved calculation of phase relations and major element partitioning related to partial melting of the mantle to 3 GPa. *Geochem Geophys Geosyst* 3:1030–1065
- Ginibre C, Kronz A, Wörner G (2002a) High-resolution quantitative imaging of plagioclase composition using accumulated back-scattered electron images: new constraints on oscillatory zoning. *Contrib Mineral Petrol* 142:436–448
- Ginibre C, Wörner G, Kronz A (2002b) Minor- and trace-element zoning in plagioclase: implications for magma chamber processes at Paríacota volcano, northern Chile. *Contrib Mineral Petrol* 143:300–315
- Glazner AF (1984) Activities of olivine and plagioclase components in silicate melts and their application to geothermometry. *Contrib Mineral Petrol* 88:260–268
- Gregory RT, Criss RE (1986) Isotopic exchange in open and closed systems. In: Valley JW, Taylor Jr. HP, O’Neil JR (eds) Stable isotopes in high temperature geological processes. *Rev Min* 16:91–127
- Guntoro A (1999) The formation of the Makassar Strait and the separation between SE Kalimantan and SW Sulawesi. *J Asian Earth Sci* 17:79–98
- Hamilton WB (1979) Tectonics of the Indonesian region. *US Geol Surv Prof Pap* 1078:345
- Hammer JE, Cashman KV, Hoblitt RP, Newman S (1999) Degassing and microlite crystallization during pre-climactic events of the 1991 eruption of Mt. Pinatubo, Philippines. *Bull Volcanol* 60:355–380
- Handley HK, Macpherson CG, Davidson JP, Berlo K, Lowry D (2007) Constraining fluid and sediment contributions to subduction-related magmatism in Indonesia: Ijen volcanic complex. *J Petrol* 48:1155–1183
- Handley HK, Davidson JP, Macpherson CG, Stimac JA (2008) Untangling differentiation in arc lavas: constraints from unusual minor and trace element variations at Salak Volcano, Indonesia. *Chem Geol* 255:360–376
- Handley HK, MacPherson CG, Davidson JP (2010) Geochemical and Sr–O isotopic constraints on magmatic differentiation at Gede Volcanic Complex, West Java, Indonesia. *Contrib Mineral Petrol* 159:885–908
- Harmon RS, Gerbe M-C (1992) The 1982–83 eruption at Galunggung volcano, Java (Indonesia): oxygen isotope geochemistry of a chemically zoned magma chamber. *J Petrol* 33:585–609
- Harmon RS, Hoefs J (1995) Oxygen isotope heterogeneity of the mantle deduced from global ¹⁸O systematics of basalts from different tectonic settings. *Contrib Mineral Petrol* 120:95–114
- Harris C, Vogeli J (2010) Oxygen isotope composition of garnet in the Peninsula Granite, Cape Granite Suite, South Africa: constraints on melting and emplacement mechanisms. *South Afr J Geol* 113:401–412
- Harris C, Smith HS, le Roex AP (2000) Oxygen isotope composition of phenocrysts from Tristan da Cunha and Gough Island lavas: variation with fractional crystallization and evidence for assimilation. *Contrib Mineral Petrol* 138:164–175
- Harris C, Pronost JJM, Ashwal LD, Cawthorn RG (2005) Oxygen and hydrogen isotope stratigraphy of the Rustenburg Layered Suite, Bushveld Complex: constraints on crustal contamination. *J Petrol* 46:579–601
- Hattori K, Sato H (1996) Magma evolution recorded in plagioclase zoning in 1991 Pinatubo eruption products. *Am Mineral* 81:982–994
- Higgins MD (1996) Crystal size distributions and other quantitative textural measurements in lavas and tuff from Egmont volcano (Mt. Taranaki), New Zealand. *Bull Volcanol* 58:194–204
- Higgins MD (2000) Measurement of crystal size distributions. *Am Mineral* 85:1105–1116
- Higgins MD (2006) Quantitative textural measurements in igneous and metamorphic petrology. Cambridge University Press, Cambridge, p 265

- Higgins MD, Roberge J (2007) Three magmatic components in the 1973 eruption of Eldfell volcano, Iceland: evidence from plagioclase crystal size distribution (CSD) and geochemistry. *J Volcanol Geotherm Res* 161:247–260
- Hildner E, Klügel A, Hauff F (2011) Magma storage and ascent during the 1995 eruption of Fogo, Cape Verde Archipelago. *Contrib Mineral Petrol* 162:751–772
- Hildreth W, Moorbath S (1988) Crustal contributions to arc magmatism in the Andes of central Chile. *Contrib Mineral Petrol* 98:455–489
- Hilton DR, Craig H (1989) A helium isotope transect along the Indonesian archipelago. *Nature* 342:906–908
- Hoefs J (2005) Stable isotope geochemistry. Springer, Berlin, p 285
- Holness MB (2005) Spatial constraints on magma chamber replenishment events from textural observations of cumulates: the Rum Layered Intrusion, Scotland. *J Petrol* 46:1585–1601
- Homma F (1932) Über das Ergebnis von Messungen an zonaren Plagioklasen aus Andesiten mit Hilfe des Universaldrehtisches. *Schweiz Mineral Petrogr Mitt* 12:345–351
- Housh TB, Luhr JF (1991) Plagioclase-melt equilibria in hydrous systems. *Am Mineral* 76:477–492
- Humphreys MCS, Blundy JD, Sparks RSJ (2006) Magma evolution and open-system processes at Shiveluch volcano: insights from phenocryst zoning. *J Petrol* 47:2303–2334
- Humphreys MCS, Blundy JD, Sparks RSJ (2008) Shallow-level decompression crystallisation and deep magma supply at Shiveluch Volcano. *Contrib Mineral Petrol* 155:45–61
- Humphreys MCS, Christopher T, Hards V (2009) Microlite transfer by disaggregation of mafic inclusions following magma mixing at Soufrière Hills volcano, Montserrat. *Contrib Mineral Petrol* 157:609–624
- Huppert HE, Sparks RSJ (1980) The fluid dynamics of a basaltic magma chamber replenished by influx of hot, dense ultrabasic magma. *Contrib Mineral Petrol* 75:279–289
- Huppert HE, Sparks RSJ (1984) Double diffusive convection due to crystallization in magmas. *Annu Rev Earth Planet Sci Lett* 12:11–37
- Ito E, White WM, Göpel C (1987) The O, Sr, Nd and Pb isotope geochemistry of MORB. *Chem Geol* 62:157–176
- Jeffery A, Gertisser R, Humaida H, O'Driscoll B, Tindle A (2010) Lava dome extrusion into an active crater lake: the 2007–2008 eruption of Kelut volcano, Java, Indonesia. Abstract—cities on Volcanoes 6, Tenerife, Spain, 31 May–4 June 2010
- Kelley KA, Plank T, Newman S, Stolper EM, Grove TL, Parman S, Hauri EH (2010) Mantle melting as a function of water content beneath the Mariana arc. *J Petrol* 51:1711–1738
- Kudo AM, Weill DF (1970) An igneous plagioclase thermometer. *Contrib Mineral Petrol* 25:52–65
- Kuo LC, Kirkpatrick RJ (1982) Pre-eruption history of phyric basalts from DSDP legs 45 and 46: evidence from morphology and zoning patterns in plagioclase. *Contrib Mineral Petrol* 79:13–27
- Kyser TK, O'Neil JR, Carmichael ISE (1981) Oxygen isotope thermometry of basic lavas and mantle nodules. *Contrib Mineral Petrol* 77:11–23
- Landi P, Métrich N, Bertagnini A, Rosi M (2004) Dynamics of magma mixing and degassing recorded in plagioclase at Stromboli (Aeolian Archipelago, Italy). *Contrib Mineral Petrol* 147:213–227
- Lange RA, Frey HM, Hector J (2009) A thermodynamic model for the plagioclase-liquid hygrometer/thermometer. *Am Mineral* 94:494–506
- Lavigne F, Thouret J-C, Hadmoko DS, Sukatja CB (2007) Lahars in Java: initiations, dynamics, hazard assessment and deposition processes. *Forum Geografi* 21:17–32
- Le Maitre RW (ed) (1989) A classification of igneous rocks and glossary of terms. Blackwell Scientific, Oxford, p 193
- Leake BE, Woolley AR, Arps CES, Birch WD, Gilbert MC, Grice JD, Hawthorne FC, Kato A, Kisch HJ, Krivovichev VG, Linthout K, Laird J, Mandarino JA, Maresch WV, Nickel EH, Rock NMS, Schumacher JC, Smith DC, Stephenson NCN, Ungaretti L, Whittaker EJW, Youzhi G (1997) Nomenclature of amphiboles: report of the subcommittee on amphiboles of the international mineralogical association, commission on new minerals and mineral names. *Can Mineral* 35:219–246
- Lesage P, Suroño (1995) Seismic precursors of the February 10, 1990 eruption of Kelut volcano, Java. *J Volcanol Geotherm Res* 65:135–146
- Longpré MA, Troll VR, Hansteen TH (2008) Upper mantle magma storage and transport under a Canarian shield-volcano, Teno, Tenerife (Spain). *J Geophys Res* 113:B08203
- Loomis TP (1979) An empirical model for plagioclase equilibrium in hydrous melts. *Geochim Cosmochim Acta* 43:1753–1759
- Lundgaard KL, Tegner C (2004) Partitioning of ferric and ferrous iron between plagioclase and silicate melt. *Contrib Mineral Petrol* 147:470–483
- Marsh BD (1988) Crystal size distribution (CSD) in rocks and the kinetics and dynamics of crystallization, I. Theory. *Contrib Mineral Petrol* 99:277–291
- Marsh BD (1998) On the interpretations of crystal size distributions in magma systems. *J Petrol* 39:553–599
- Martel C, Bourdier JL, Pichavant M, Traineau H (2000) Textures, water content and degassing of silicic andesites from recent plinian and dome-forming eruptions of Mount Pelée volcano (Martinique, Lesser Antilles). *J Volcanol Geotherm Res* 96:191–206
- Martin D, Griffiths RW, Campbell IH (1987) Compositional and thermal convection in magma chambers. *Contrib Mineral Petrol* 96:465–475
- Martin VM, Holness MB, Pyle DM (2006) Textural analysis of magmatic enclaves from the Kameni Islands, Santorini, Greece. *J Volcanol Geotherm Res* 154:89–102
- Mock A, Jerram D (2005) Crystal size distributions (CSDs) in three dimensions: insights from the 3D reconstruction of a highly porphyritic rhyolite. *J Petrol* 46:1525–1541
- Mollo S, Del Gaudio P, Ventura G, Iezzi G, Scarlato P (2010) Dependence of clinopyroxene composition on cooling rate in basaltic magmas: implications for thermobarometry. *Lithos* 118:302–312
- Mollo S, Putirka K, Iezzi G, Del Gaudio P, Scarlato P (2011) Plagioclase-melt (dis)equilibrium due to cooling dynamics: implications for thermometry, barometry and hygrometry. *Lithos* 125:221–235
- Morgan DJ, Jerram DA (2006) On estimating crystal shape for crystal size distribution analysis. *J Volcanol Geotherm Res* 154:1–7
- Morgan DJ, Jerram DA, Chertkoff DG, Davidson JP, Pearson DG, Kronz A, Nowell GM (2007) Combining CSD and isotopic microanalysis: magma supply and mixing processes at Stromboli Volcano, Aeolian Islands, Italy. *Earth Planet Sci Lett* 260:419–431
- Morimoto N, Fabries J, Ferguson AK, Ginzburg IV, Ross M, Seifert FA, Zussman J, Aoki K, Gottardi G (1988) Nomenclature of pyroxenes. *Mineral Mag* 52:535–550
- Nakagawa M, Wada K, Wood CP (2002) Mixed magmas, mush chambers and eruption triggers: evidence from zoned clinopyroxene phenocrysts in andesitic scoria from the 1995 eruptions of Ruapehu volcano, New Zealand. *J Petrol* 43:2279–2303
- Nelson ST, Montana A (1992) Sieve-textured plagioclase in volcanic rocks produced by rapid decompression. *Am Mineral* 77:1242–1249
- Newcomb KR, McCann WR (1987) Seismic history and seismotectonics of the Sunda arc. *J Geophys Res* 92:421–439
- Nimis P (1995) A clinopyroxene geobarometer for basaltic systems based on crystal-structure modelling. *Contrib Mineral Petrol* 121:115–125

- Nimis P, Taylor WR (2000) Single clinopyroxene thermobarometry for garnet peridotites. part I. Calibration and testing of a Cr-in-Cpx barometer and an enstatite-in-Cpx thermometer. *Contrib Mineral Petrol* 139:541–554
- O'Driscoll B, Donaldson CH, Troll VR, Jerram DA, Emeleus CH (2007) An origin for harrisitic and granular olivine in the Rum Layered Suite, NW Scotland: a crystal size distribution study. *J Petrol* 48:253–270
- Pearce TH, Kolisnik AM (1990) Observations of plagioclase zoning using interference imaging. *Earth Sci Rev* 29:9–26
- Platz T, Cronin SJ, Cashman KV, Stewart RB, Smith IEM (2007) Transition from effusive to explosive phases in andesite eruptions—a case study from the AD1655 eruption of Mt. Taranaki, New Zealand. *J Volcanol Geotherm Res* 161:15–34
- Preece K, Barclay J, Gertisser R, Herd RA (2013a) Textural and micro-petrological variations in the eruptive products of the 2006 dome-forming eruption of Merapi volcano, Indonesia: implications for sub-surface processes. *J Volcanol Geotherm Res*. doi:10.1016/j.jvolgeores.2013.02.006
- Preece K, Gertisser R, Berlo K, Barclay J, Herd R (2013b) Volatile and light lithophile trace element geochemistry of the 2010 eruption of Merapi volcano revealed by melt inclusions. Abstract—International Association of Volcanology and Chemistry of the Earth's Interior (IAVCEI) Scientific Assembly, Kagoshima, Japan, 20–24 July 2013
- Price RC, Gamble JA, Smith IEM, Stewart RB, Eggers S, Wright IC (2005) An integrated model for the temporal evolution of andesites and rhyolites and crustal development in New Zealand's North Island. *J Volcanol Geotherm Res* 140:1–24
- Putirka KD (2005) Igneous thermometers and barometers based on plagioclase + liquid equilibria: tests of some existing models and new calibrations. *Am Mineral* 90:336–346
- Putirka KD (2008) Thermometers and barometers for volcanic systems. *Rev Mineral Geochem* 69:61–120
- Putirka KD, Mikaelian H, Ryerson F, Shaw H (2003) New clinopyroxene-liquid thermobarometers for mafic, evolved, and volatile-bearing lava compositions, with applications to lavas from Tibet and the Sanke River Plain, Idaho. *Am Mineral* 88:1542–1554
- Reubi O, Blundy J (2008) Assimilation of plutonic roots, formation of high-K 'exotic' melt inclusions and genesis of andesitic magmas at Volcán De Colima, Mexico. *J Petrol* 49:2221–2243
- Reubi O, Nicholls IA, Kamenetsky VS (2002) Early mixing and mingling in the evolution of basaltic magmas: evidence from phenocryst assemblages, Slamet volcano, Java, Indonesia. *J Volcanol Geotherm Res* 119:255–274
- Ridolfi F, Renzulli A, Puerini M (2010) Stability and chemical equilibrium of amphibole in calc-alkaline magmas: an overview, new thermobarometric formulations and applications to subduction-related volcanoes. *Contrib Mineral Petrol* 160:45–66
- Roggensack K, Hervig RL, McKnight SB, Williams SN (1997) Explosive basaltic volcanism from Cerro Negro volcano: influence of volatiles on eruptive style. *Science* 277:1639–1642
- Ruprecht P, Wörner G (2007) Variable regimes in magma systems documented in plagioclase zoning patterns: El Misti stratovolcano and Andahua monogenetic cones. *J Volcanol Geotherm Res* 165:142–162
- Savov IP, Luhr JF, Navarro-Ochoa C (2008) Petrology and geochemistry of lava and ash erupted from Volcán Colima, Mexico, during 1998–2005. *J Volcanol Geotherm Res* 174:241–256
- Schwarz S, Klügel A, Wohlgenuth-Ueberwasser C (2004) Melt extraction pathways and stagnation depths beneath the Madeira and Desertas rift zones (NE Atlantic) inferred from barometric studies. *Contrib Mineral Petrol* 147:228–240
- Shcherbakov VD, Plechov PY, Izbekov PE, Shipman JS (2010) Plagioclase zoning as an indicator of magma processes at Bezymianny Volcano, Kamchatka. *Contrib Mineral Petrol* 162:83–99
- Shore M, Fowler AD (1996) Oscillatory zoning in minerals: a common phenomenon. *Can Mineral* 34:1111–1126
- Siebert L, Simkin T, Kimberly P (2011) *Volcanoes of the world*, 3rd edn. University of California Press, Los Angeles, p 551
- Silver EA, Reed D, McCaffrey R (1983) Back arc thrusting in the eastern Sunda arc, Indonesia: a consequence of arc-continent collision. *J Geophys Res* 88:7429–7448
- Singer BS, Dungan MA, Layne GD (1995) Textures and Sr, Ba, Mg, Fe, K and Ti compositional profiles in volcanic plagioclase: clues to the dynamics of calc-alkaline magma chambers. *Am Mineral* 80:776–798
- Sisson TW, Layne GD (1993) H₂O in basalt and basaltic andesite glass inclusions from four subduction-related volcanoes. *Earth Planet Sci Lett* 117:619–635
- Smyth H, Hall R, Hamilton J, Kinny P (2005) In: East Java: Cenozoic basins, volcanoes and ancient basement. Proceedings, Indonesian Petroleum Association, thirtieth annual convention and exhibition, pp 251–266
- Smyth HR, Hamilton PJ, Hall R, Kinny PD (2007) The deep crust beneath island arcs: inherited zircons reveal a Gondwana continental fragment beneath East Java, Indonesia. *Earth Planet Sci Lett* 258:269–282
- Snyder D, Tait S (1995) Replenishment of magma chambers: comparison of fluid-mechanic experiments with field relations. *Contrib Mineral Petrol* 122:230–240
- Sparks RSJ, Sigurdsson H, Wilson L (1977) Magma mixing: a mechanism of triggering acid explosive eruptions. *Nature* 267:315–318
- Stewart ML, Fowler AD (2001) The nature and occurrence of discrete zoning in plagioclase from recently erupted andesitic volcanic rocks, Montserrat. *J Volcanol Geotherm Res* 106:243–253
- Stronck NA, Klügel A, Hansteen TH (2009) The magmatic plumbing system beneath El Hierro (Canary Islands): constraints from phenocrysts and naturally quenched basaltic glasses in submarine rocks. *Contrib Mineral Petrol* 157:593–607
- Sugawara T (2001) Ferric iron partitioning between plagioclase and silicate liquid: thermodynamics and petrological applications. *Contrib Mineral Petrol* 141:659–686
- Sun S, McDonough WF (1989) Chemical and isotopic systematics of ocean basins: implications for mantle composition and processes. In: Saunders AD, Norry MJ (eds) *Magmatism in the Ocean Basins*, *Geol Soc Lond Spec Publ* 42:313–346
- Sunagawa I (1992) In situ investigation of nucleation, growth and dissolution of silicate crystals at high temperatures. *Annu Rev Earth Planet Sci* 20:113–142
- Taylor HP, Sheppard SMF (1986) Igneous rocks: I. Processes of isotopic fractionation and isotope systematics. In: Valley JW, Taylor Jr. HP, O'Neil JR (eds) *Stable isotopes in high temperature geological processes*. *Rev Min* 16:227–271
- Tepley FJ, Davidson JP, Tilling RI, Arth JG (2000) Magma mixing, recharge and eruption histories recorded in plagioclase phenocrysts from El Chichón volcano, Mexico. *J Petrol* 41:1397–1411
- Thouret J-C, Abdurachman KE, Bourdier J-L, Bronto S (1998) Origin, characteristics and behaviour of lahars following the 1990 eruption of Kelud volcano, eastern Java (Indonesia). *B Volcanol* 59:460–480
- Troll VR, Schmincke H-U (2002) Magma mixing and crustal recycling recorded in ternary feldspar from compositionally zoned peralkaline ignimbrite 'A', Gran Canaria, Canary Islands. *J Petrol* 43:243–270
- Troll VR, Donaldson CH, Emeleus CH (2004) Pre-eruptive magma mixing in ash-flow deposits of the Tertiary Rum Igneous Centre, Scotland. *Contrib Mineral Petrol* 147:722–739
- Troll VR, Hilton DR, Jolis EM, Chadwick JP, Blythe LS, Deegan FM, Schwarzkopf LM, Zimmer M (2012) Crustal CO₂ liberation

- during the 2006 eruption and earthquake events at Merapi volcano, Indonesia. *Geophys Res Lett* 39:L11302
- Troll VR, Deegan FM, Jolis EM, Harris C, Chadwick JP, Gertisser R, Schwarzkopf LM, Borisova A, Bindeman IN, Sumarti S, Preece K (2013) Magmatic differentiation processes at Merapi volcano: inclusion petrology and oxygen isotopes. *J Volcanol Geotherm Res*. doi:10.1016/j.jvolgeores.2012.11.001
- Tsuchiyama A (1985) Dissolution kinetics of plagioclase in the melt of the system diopside-albite-anorthite and origin of dusty plagioclase in andesites. *Contrib Mineral Petrol* 89:1–16
- Turner JS, Campbell IH (1986) Convection and mixing in magma chambers. *Earth Sci Rev* 23:255–352
- Valley JW (1986) Stable isotope geochemistry of metamorphic rocks. *Rev Mineral Geochem* 16:445–489
- van Bemmelen RW (1949) The geology of Indonesia, vol 1A. Government Printing Office, The Hague, p 732
- van Bergen MJ, Bernard A, Sumarti S, Sriwana T, Sitorus K (2000) Crater lakes of Java: Dieng, Kelud, Ijen. Excursion Guidebook—International Association of Volcanology and Chemistry of the Earth's Interior (IAVCEI) General Assembly, Bali 2000, p 42
- Vance J (1962) Zoning in igneous plagioclase; normal and oscillatory zoning. *Am J Sci* 260:746–760
- Vennemann TW, Smith HS (1990) The rate and temperature of reaction of CLF_3 with silicate minerals, and their relevance to oxygen isotope analysis. *Chem Geol* 86:83–88
- Vinet N, Higgins MD (2011) What can crystal size distributions and olivine compositions tell us about magma solidification processes inside Kilauea Iki lava lake, Hawaii? *J Volcanol Geotherm Res* 208:136–162
- Wallace PJ (2005) Volatiles in subduction zone magmas: concentrations and fluxes based on melt inclusion and volcanic gas data. *J Volcanol Geotherm Res* 140:217–240
- Widiyantoro S, van der Hilst R (1996) Structure and evolution of lithospheric slab beneath the Sunda arc, Indonesia. *Science* 271:1566–1570
- Wiesmaier S, Deegan FM, Troll VR, Carracedo JC, Chadwick JP, Chew DM (2011) Magma mixing in the 1100 AD Montaña Reventada composite lava flow, Tenerife, Canary Islands: interaction between rift zone and central volcano plumbing systems. *Contrib Mineral Petrol* 162:651–669
- Wilke M, Behrens H (1999) The dependence of the partitioning of iron and europium between plagioclase and hydrous tonalitic melt on oxygen fugacity. *Contrib Mineral Petrol* 137:102–114
- Wirakusumah AD (1991) Some studies of the volcanology, petrology and structure of Mt. Kelut, East Java, Indonesia. PhD Thesis, Victoria University, Wellington, p 460
- Worster MG, Huppert HE, Sparks RSJ (1990) Convection and crystallization in magma cooled from above. *Earth Planet Sci Lett* 101:78–89

Copyright of Contributions to Mineralogy & Petrology is the property of Springer Science & Business Media B.V. and its content may not be copied or emailed to multiple sites or posted to a listserv without the copyright holder's express written permission. However, users may print, download, or email articles for individual use.